AN ABSTRACT OF THE THESIS OF

Ali Alnahit for the degree of Master of Science in Civil Engineering presented on June 16, 2015.

Title: A Remotely Controlled Siphon System for Dynamic Water Storage Management

Abstract approved: _____

Arturo S. Leon

This thesis presents an analytical, experimental and numerical study of the initiation of flows in a siphon for rapid and gradual openings of a downstream valve. Three initial water levels in the upstream tank and four final positions for the downstream valve were investigated. Two opening times of the downstream valve were also studied. Good agreement between analytical, experimental and numerical results were obtained. The proposed siphon system was found to initiate the flow regardless the downstream valve is opened gradually or rapidly. However, small leakages may lead to air at atmospheric pressure to rush into the top of the siphon and stop the flow. Overall, the proposed siphon system can be an effective and inexpensive method to dynamically manage the storage of ponds and wetlands for flood control.

A Remotely Controlled Siphon System for Dynamic Water Storage Management

by

Ali Alnahit

A THESIS

submitted to

Oregon State University

in partial fulfillment of
the requirements for the
degree of

Master of Science

Presented June 16, 2015
Commencement June 2016

Master of Science thesis of Ali Alnahit presented on June 16, 2015.

APPROVED:

_____

Major Professor, representing Civil Engineering

_____

Head of the School of Civil and Construction Engineering

_____

Dean of the Graduate School

I understand that my thesis will become part of the permanent collection of Oregon State University libraries. My signature below authorizes release of my thesis to any reader upon request.

_____

Ali Alnahit, Author

ACKNOWLEDGEMENTS

First and foremost, I would like to express my gratitude to my advisor, Dr. Arturo S. Leon, for his support, guidance, and encouragement throughout my graduate studies. His technical advice was essential to the completion of this thesis and has taught me innumerable lessons in hydraulics and academic research in general.

Dr. Ali Nikukar, I would like to thank you for your inspiration and encouragement to pursuit my master's degree. Without your support, this achievement would not have been possible.

I would like to thank all of my family and friends for their support during my graduate studies. Through all of their encouragement, moral support, and edible support, I have been enabled to complete this goal. I am especially grateful to my mother, for her wisdom, love, and support during the past couple of years. Without her continuous support and encouragement, I never would have been able to achieve my goals.

Finally, I would also like thank all of the professors and graduate students with whom I've had the pleasure of meeting and working with at Oregon State University.

TABLE OF CONTENTS

LIST OF FIGURES

LIST OF FIGURES (Continued)

LIST OF FIGURES (Continued)

LIST OF FIGURES (Continued)

LIST OF TABLES

Chapter 1: Introduction

In recent decades, the significant and rapid increase of impervious surfaces has increased the risk of flooding. The effects of flooding on the environment are extensive and significant, resulting in more loss of lives and damage to property and crops (NHC, 1997; NWS, 2013). According to Newson (1997), one-sixth of all urban land in the U.S and around 10 percent of the US population are within the 100-year flood area. The National Weather Service NWS (2013) states that direct freshwater flood damages in the U.S. in 2011 and 2012 were $3.9 and $0.5 billion, respectively. There are two common approaches to reducing flood damages: structural and nonstructural measures. The traditional approach (structural measures) can reduce inundation of the floodplain in several ways. For instance, reservoirs reduce downstream peak flow rates, levees and flood walls confine the flow of the rivers, and floodways help divert excess flow (ICE, 2002; De Bruijn et al., 2008; Breckpot et al., 2010). Although structural measure strategies can be effective in reducing floods effects, they have a limited capacity to mitigate floods since only small parts of the watersheds (river and floodplains) are used for flood management.

Since flooding impacts have increased in frequency and severity, there is a new emphasis on evaluating nonstructural and watershed management approaches to deter-

mine whether they are effective strategies for flood prediction, prevention and mitigation (Lamothe et al., 2005; Van Schijndel, 2006; Breckpot et al., 2010). A report from the Environmental Protection Agency (EPA, 1996) concluded that watershed approaches are the most effective approaches to address water resource challenges. In watershed management, all characteristics of a watershed can be linked to the goal of management and therefore flooding in one area can be linked to development upstream. This approach can help to maintain and mimic the natural hydrology system (Buss, 2005).

Within a watershed, ponds and wetlands can play an important role in flood reduction, increasing water quality, and creating habitats for fauna (Hey and Philippi, 1995; Mitsch and Day, 2006; Lemke and Richmond, 2009). Ponds and wetlands also could increase flood storage by storing, holding, and percolating water (Wharton, 1970; Hwang et al., 1977; Costanza et al., 1989; Godschalk, 1999; Cole et al., 1997; Erwin, 2009; Babbar-Sebens et al., 2013). A study demonstrated that wetlands are able to absorb and hold greater amounts of floodwater than previously thought (Godschalk, 1999). Based on an experiment that involved constructing ponds along the Des Plaines River in Illinois, it was found that a marsh of only 5.7 acres could retain the natural run-off of a 410-acre watershed. This study estimated that only 13 million acres of wetlands (3% of the upper Mississippi watershed) would have been needed to prevent the catastrophic flood of 1993 (Godschalk, 1999). Other studies also show the effectiveness of using wetlands for flood mitigation (Bekele and Nicklow, 2007; Babbar-Sebens et al.,

2013). A report of the United Nations (UNDP and UNISDR, 2006) concluded that upland wetlands could be effective for small floods, but for large floods their value may be greatly reduced as their storage capacity may be exceeded. However, wetland areas and available storage volumes have decreased significantly in the last two centuries due to population growth and extensive land use (Wharton, 1970; Hwang et al., 1977; Costanza et al., 1989; Godschalk, 1999; Cole et al., 1997; Erwin, 2009; Babbar-Sebens et al., 2013). Thus, the limited availability of natural ponds and the increase of flood frequency make intelligent management of ponds necessary to help mitigate floods. A potential solution for this problem could be to release water from ponds ahead of (e.g., few days before) a heavy rainfall event that is forecasted to produce flooding. The water released would increase the available storage capacity and hence reduce the impact of flooding.

In order to release water from ponds, a remotely controlled siphon system could be used. As part of this research, an innovative siphon system was designed and built (Figure 1.1). This system 1) would not require any construction except a simple anchoring of the siphon pipe for safety; (2) could be remotely operated using a SCADA-type control and can be activated through direct radio, via satellite, wireless radio or a combination of these communications channels, (3) would not need significant energy except for keeping the siphon pipe full and for actuating (opening and closing) the downstream valve. For this small requirement of energy, a small solar panel could be used. This new system could be used by flood control managers to remotely open and close hundreds or

thousands simultaneously.
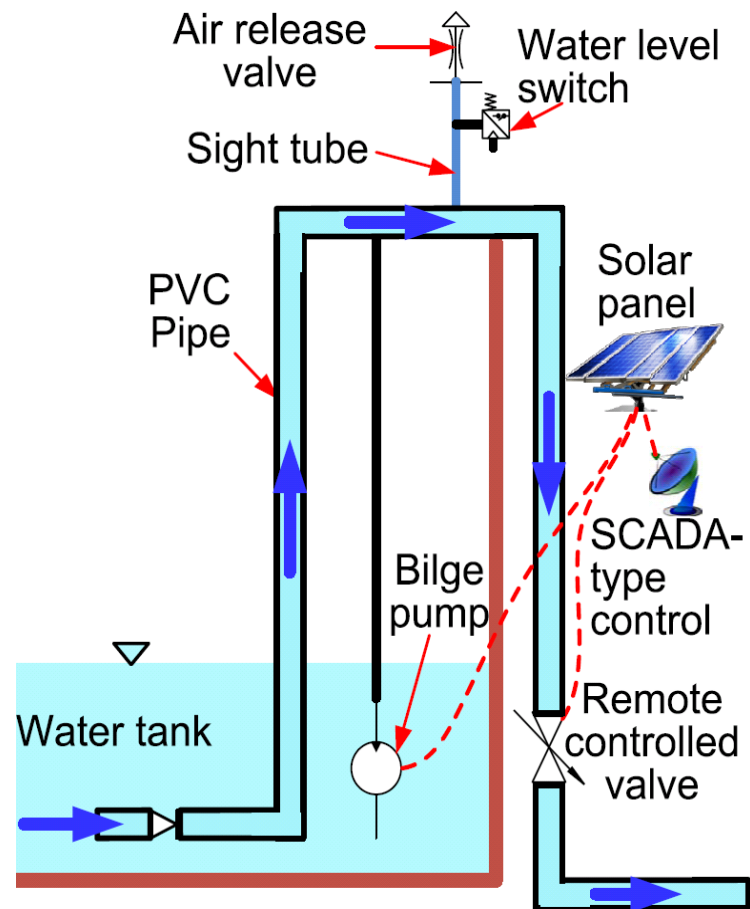
Figure 1.1: Schematic of siphon system design

Siphon Flows

Siphons have been known since early times as simple and inexpensive devices for transferring water using gravitational force (Newman and Searle, 1949; Potter and Barnes, 1971; Garrett, 1991; Hughes, 2010). Siphons work due to the difference in pressure between the top of the siphon (negative pressure) and the atmospheric pressure at the upper reservoir. This device can effe ctively remove water from reservoirs and ponds in remote locations without access to electricity and provide an increased capacity of storage in emergency situations. When set up properly, siphons usually require minimal oversight. However, they are limited by the height of lift from the reservoir to the crest of the pond and the maximum drawdown of wate (Lombardi, 1996; Morrison-Maierle, 2012).

Considerable research has been conducted on siphon flow (Newman and Searle, 1949; Potter and Barnes, 1971; Garrett, 1991; Hughes, 2010; Binder and Richert, 2011). Govi (1989) and Cambiaghi and Schuster (1989) introduced a new system using siphon principle as an emergency drainage treatment for landslides. Bryant (1996) tested the hydraulic performance of a siphon system used to drain a small earthen dam, where comparisons were made between theoretical siphon hydraulic performance and actual field performance. Leumas (1998) discussed the variables that should be considered in designing siphons and repairs to existing dams. Recently, siphon drainage combined with electropneumatic drainage has been the method for discharging ground water in Europe,

especially in France (Clark et al., 2007; Bomont, 2008; Mrvik and Bomont, 2012).

Several studies exist which have focused on the maximum height limit of siphon drainage and the maintenance of siphon and management requirements (Lombardi, 1996; Zhang and Zhang, 1999; Yongfang and Yingjun, 1999; La Stabilsiation et al., 2013; Cai et al., 2014; Boatwright, 2014). Although there is vast research on siphon flows, the regulation of siphon flows using valves or gates downstream have not been fully explored yet.

This thesis aims to investigate the performance of the proposed siphon system as a method for the dynamic management of the storage of wetlands and ponds without using significant energy. To investigate the reliability of this system to initiate the flow when regulated with a valve, analytical, experimental, and three-dimensional numerical modeling work is performed. This thesis is divided as follows. First, the experimental work is presented. Second, the numerical simulations using Star CCM+ is shown. Third, the analytical solution is laid out. Fourth, the results of experimental, numerical, and analytical solution are compared. Finally, the overall results are summarized in the conclusion.

Chapter 2: Materials and Methods

2.1   Laboratory Experiments

2.1.1   Experimental Setup

Laboratory experiments were conducted to investigate a siphon system as a method for the dynamic management of water storage. These experiments consist of six components as shown in Figure 2.1: (1) an upstream tank with a diameter of 1.05 m and a height of 1.6 m; (2) 0.038 m diameter and 4.34 m long PVC pipe; (3) a check valve at the pipe inlet; (4) a submersible pump (200 galons per hour (GPH)) used to prime the pipe, if necessary; (5) an air valve used to release the air from the system when priming the pipe; (6) an actuator valve used to control the opening/closing of the downstream valve. The actuator and submersible pump are operated using a solar panel. The operation of the system and data collection are accomplished using a LabVIEW system. The prototype of the experiment is shown in Figure 2.2.
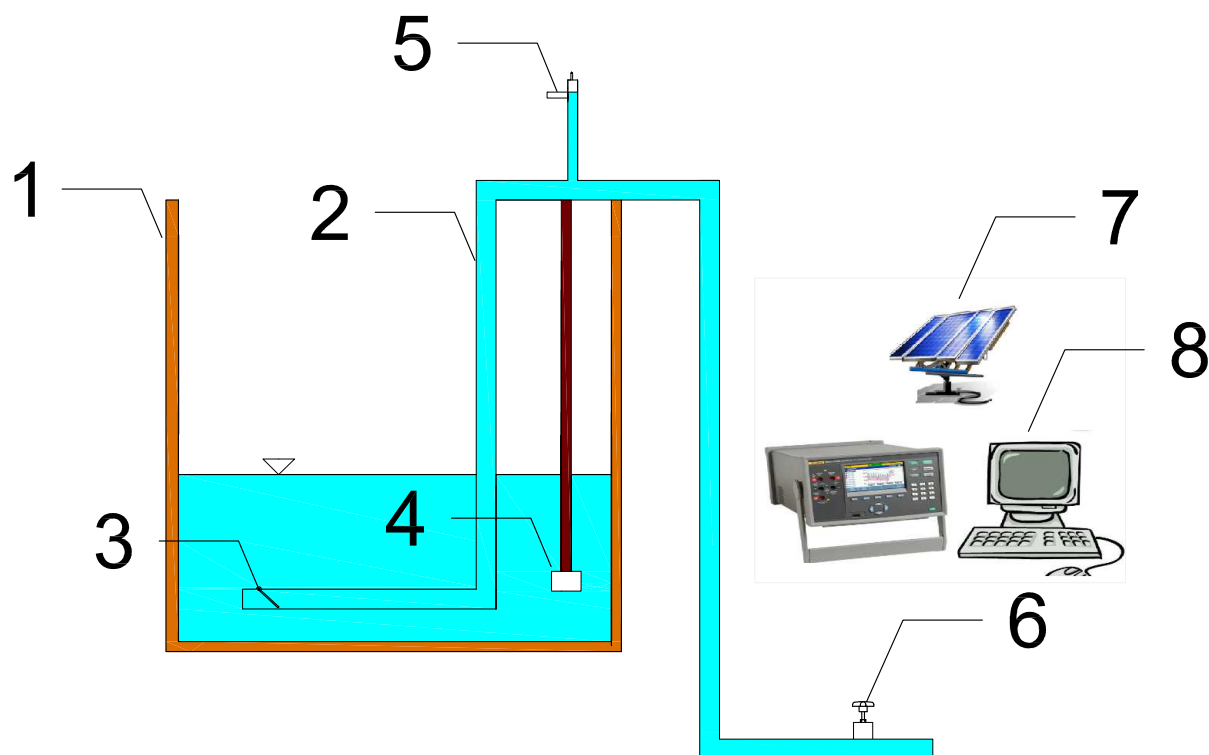
Figure 2.1: Experimental components: (1) upstream tank; (2) PVC pipe; (3) check valve ; (4) submersible pump; (5) air valve; (6) actuated valve; (7) solar panel; (8) data acquisition system.
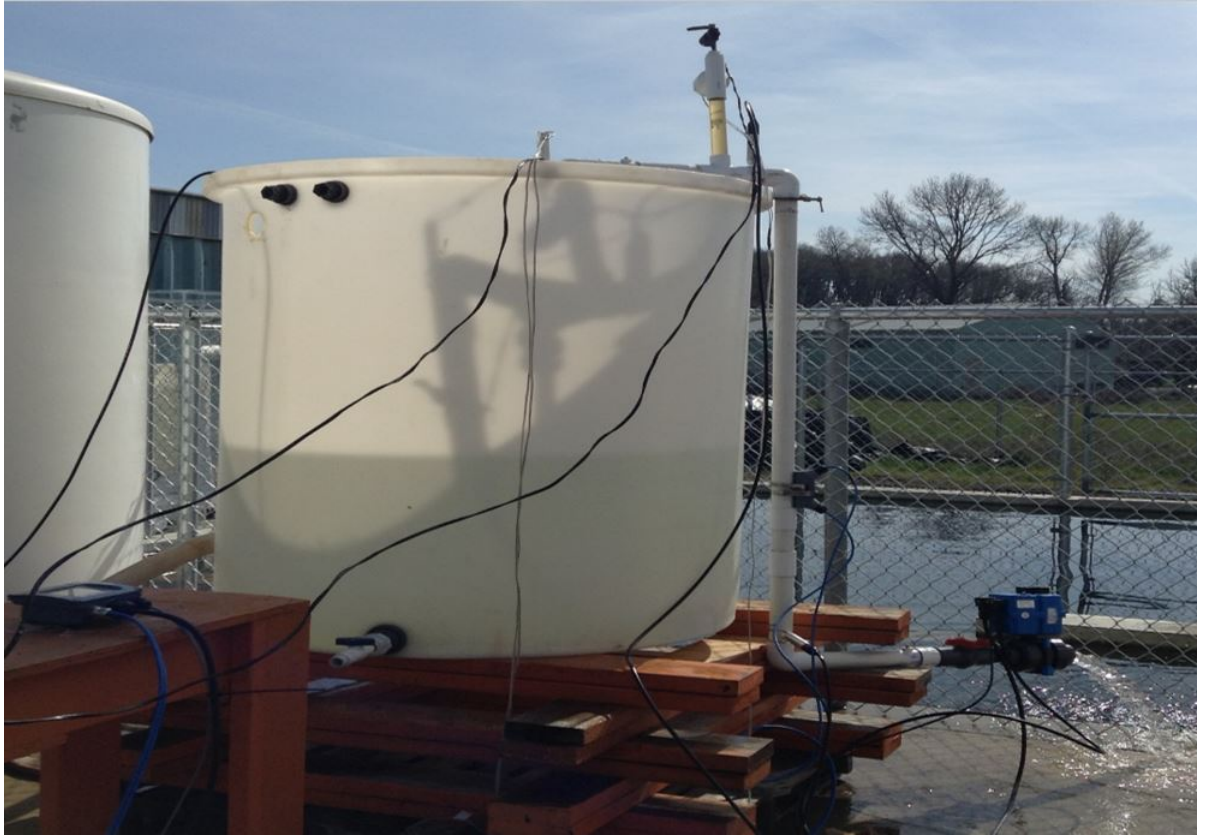
Figure 2.2: Photograph of the siphon experiment

Three pressure transducers (UNIK 5000) were installed at three different locations indicated in Figure 2.3 to measure pressures during each experiment. The discharge was measured with an electromagnetic flowmeter. The sampling rate for the pressure transducers was set to 36 Hz. An initial study yielded that this frequency introduce significant noise. All the pressure transducers had a resolution of $\pm$ 3.2 mm, and they range from 3.5 bar to 700 bar (51 to 10,000 psi).
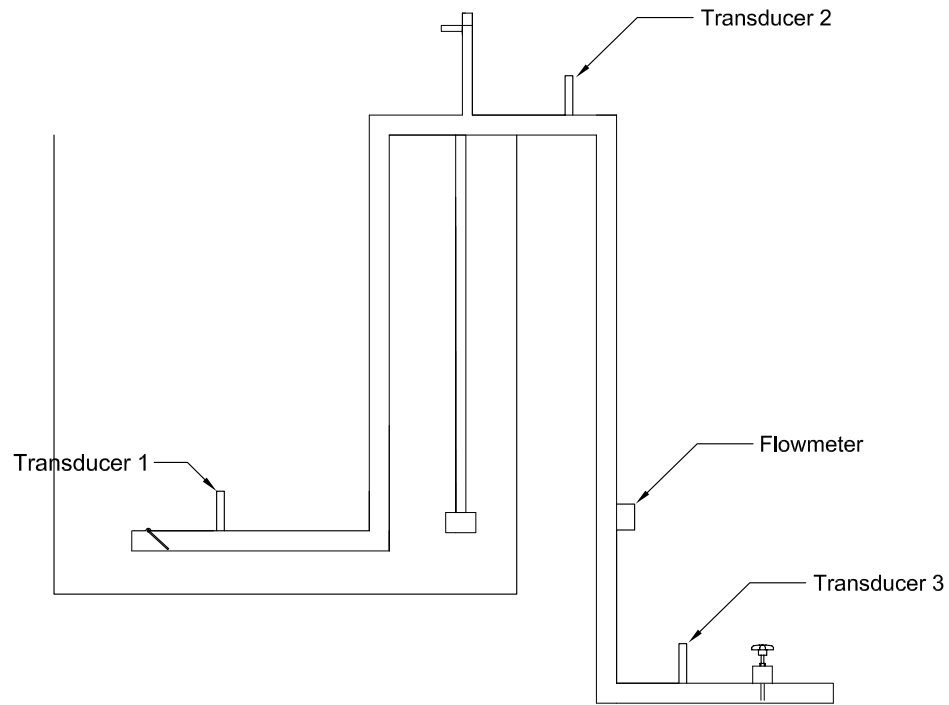
Figure 2.3: Locations of pressure transducers and flowmeter

2.1.2 Measurement Conditions

The experiments were conducted with three different initial water levels (H_A=1.14m, H_B=0.60m, and H_C=0.30m). These three different initial water levels are shown in Fig-

ure 2.4. For each water level, four different valve openings were tested (25%, 50%, 75%, and 100% of the cross-sectional area) as shown in Figure 2.5. Additionally, two times of gate opening were tested. The first time is 0.1 s, which corresponds to fast opening. The second time is 30 min, which correspond to very small opening. Finally, flow discharge and pressure measurements were made for each experiment. Every experiment was repeated at least four times to ensure consistency of the results.
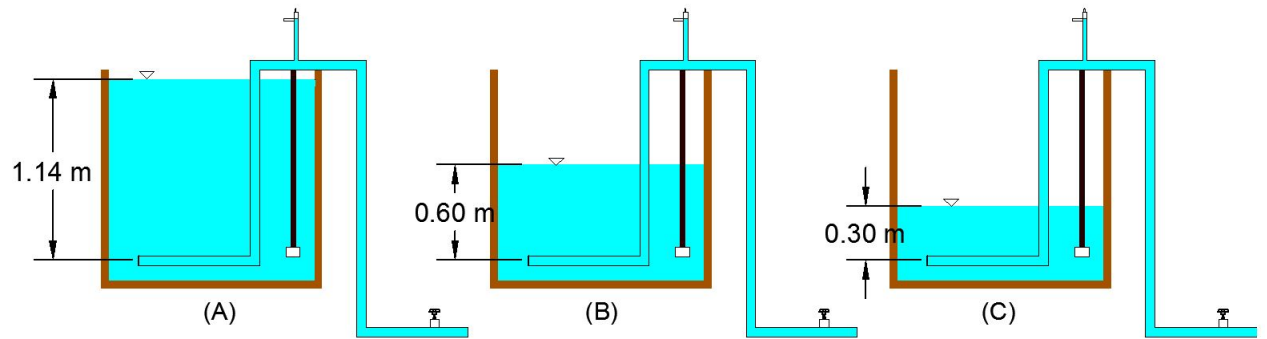
Figure 2.4: Three different water levels: (A) tank completely full; (B) tank half full; (C) tank 1/3 full
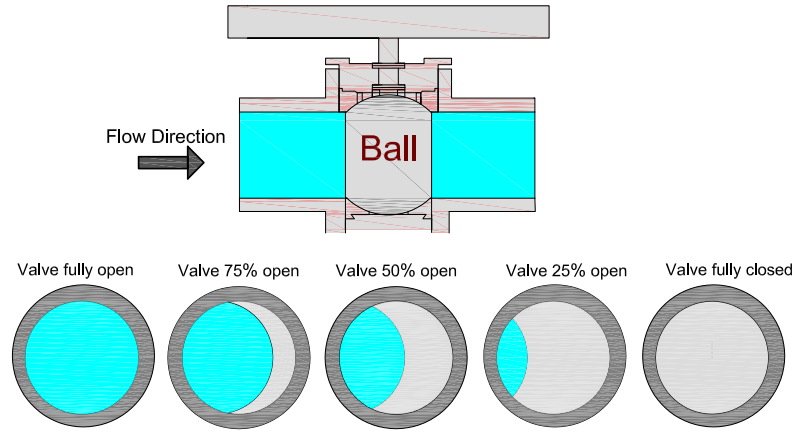
Figure 2.5: Ball valve openings (light blue indicates water)

2.1.3   Signal filtering

Filters of some sort are essential in data acquisition systems to remove selected frequencies from an incoming signal and minimize noise (Holloway, 1958). In this thesis, a low pass filter was used to smooth noisy data. The low pass filter removes the corrupting high frequency noises in the data. In order to eliminate unwanted response, the data was filtered using a Matlab generated Chebyshev low-pass filter which effectively removed frequencies above 4 Hz . The original time series and filtered data are shown in Figure 2.6

and Figure 2.7,respectively.
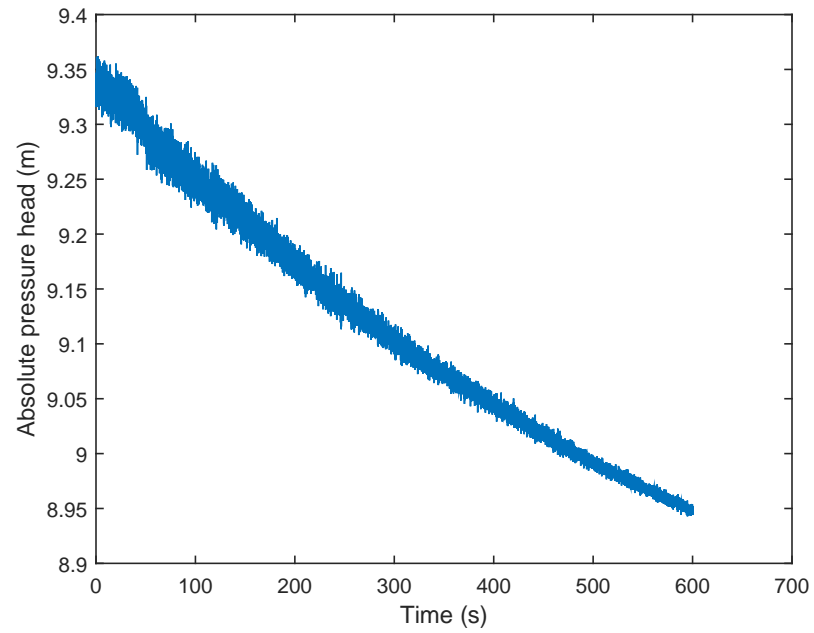
Figure 2.6: Absolute pressure head versus time when the valve is 100% opened (without filtering)
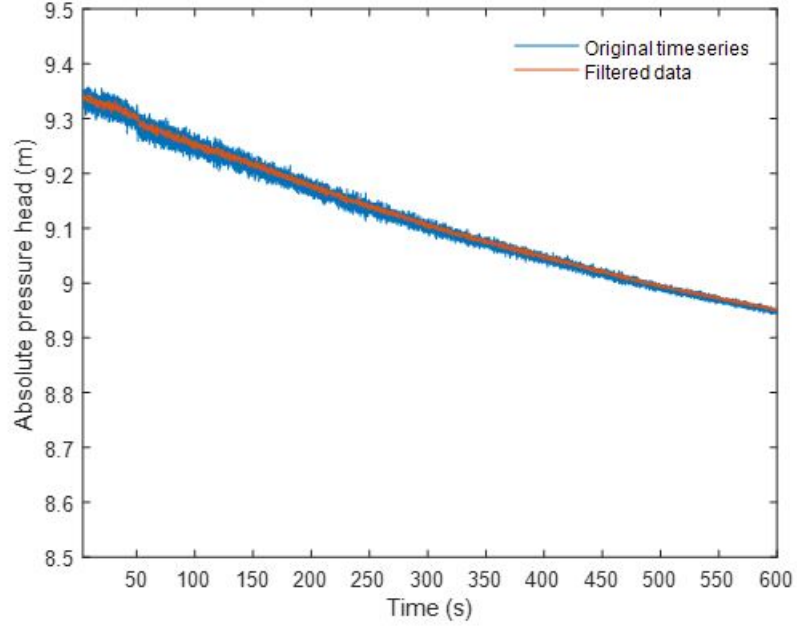
Figure 2.7: Absolute pressure head versus time when the valve is 100% opened (with filtering and without filtering)

2.2   Numerical simulations

2.2.1   Model description

Using the 3D Computational Fluid Dynamics (CFD) model Star-CCM+ v7.0 (CD-adapco, 2012), the previously described experiment was simulated. The overall process to simulate the experimental siphon flow consisted of: (1) using 3D-CAD model

(CD-adapco, 2012) to create a 3D solid geometry; (2) building the mesh; (3) selecting appropriate boundary conditions; (4) selecting the numerical model and parameters of the simulation; (5) ensuring grid convergence; and (5) visualizing the results. The parameters used in the numerical simulation are the same as those of the corresponding experiments. Three additional simulations with (H=0.8 m) and a fully opened downstream valve were performed with different grid sizes to investigate grid convergence. A brief discussion of the 3D numerical model is presented next.

2.2.2 Numerical Model

The governing conservation equations are given by (CD-adapco, 2012):

$$\frac{\partial \rho}{\partial t} + \bigtriangledown \cdot (\rho \vec{u}) = 0 \tag{2.1}$$

$$\frac{\partial \rho u}{\partial t} + \bigtriangledown \cdot (\rho \vec{u} \vec{u}) = \bigtriangledown \cdot (\mu \bigtriangledown \vec{u}) - \bigtriangledown P + \rho g \tag{2.2}$$

Where ρ = local averaged density of fluid, D = diameter, t = time, $\vec{u}$ = velocity vector μ = local averaged dynamic viscosity, P = pressure, and g = gravity.

A Volume of Fluid (VOF) model is used to simulate interface between the air and water phases. The VOF model employs an interface tracking function that indicates the fractional amount of fluid present within a control volume (Van Sint Annaland et al.,

2005) .

The transport local averaged density ρ and viscosity μ are described as following:

$$\frac{DF}{Dt} = \frac{\partial F}{\partial t} + (\vec{u} \cdot \bigtriangledown F) = 0 \qquad (2.3)$$

For the local average density ρ and viscosity μ, linear weighing of densities and viscosities of water and air is used:

$$\rho = F\rho_{air} + (1 - F)\rho_{water} \qquad (2.4)$$

$$\mu = F\mu_{air} + (1 - F)\mu_{water} \qquad (2.5)$$

The compressibility of the air phase is accounted by using the ideal gas law:

$$\rho = \frac{P_{abs}}{RT} \qquad (2.6)$$

Where P_{abs} = absolute pressure, R = gas constant, and T = temperature.

Because the flow is highly turbulent, turbulence modeling is required to predict the Reynolds stresses. In this study, turbulence is simulated using Reynolds-Averaged Navier-Stokes (RANS) turbulence model and a Realizable two-layer k-ϵ turbulence closure model (Jones and Launder, 1973; Shih et al., 1995; CD-adapco, 2012). Realizable two-layer k-ϵ model has been effective in studying industrially relevant flows (Versteeg

and Malalasekera, 2007).

2.2.3   Computational Domain

As shown in Figure 2.8, the computational domain of the numerical experiment involves two cylindrical tanks with diameters of 1.06 m and 0.80 m, respectively. The computational domain of the numerical experiment was extended beyond the outlet of the siphon represented by the second tank. This extension was made to avoid specifying a boundary condition at the outlet of the pipe. A circular pipe with a diameter of 0.0384 m connects the two tanks. To simulate different openings of the downstream ball valve in the physical experiment, various gate positions at intermediate times were specified. The latter means that incremental openings are simulated in Star-CCM+ rather than continuous as in the physical experiment.
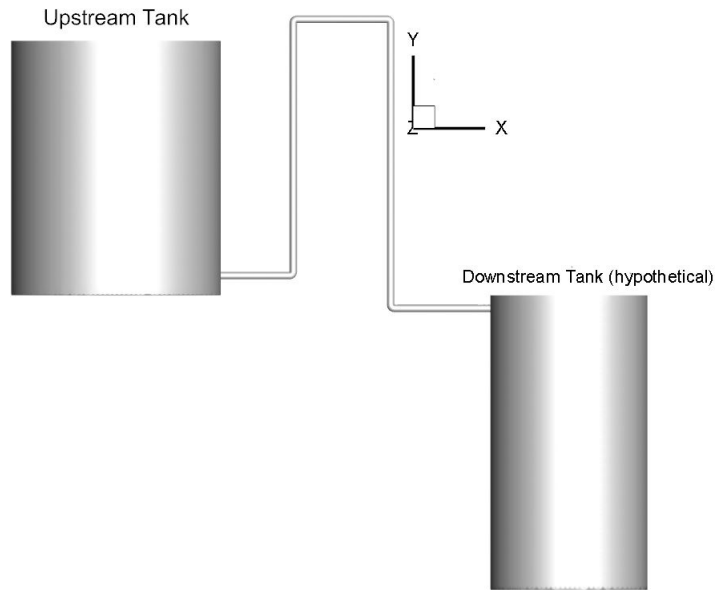
Figure 2.8: Sketch of computational domain showing the upstream and downstream tanks

2.2.4 Meshing

A trimmer grid is used to span the computational domain as shown in Figure 2.9. The mesh size is refined around the pipe inlet, outlet and the elbows using a prism layer to improve the accuracy of the flow solution. A surface wrapper is employed to refine the intersecting parts of the system (e.g, the siphon pipe with the downstream valve). The mesh sizes used for the simulations are listed in Table 2.1.

Figure 2.9: Computational mesh on surface of the tanks and surrounding the pipe region

Table 2.1: Mesh size used for different regions of the computational domain

Upstream tank (m)	Siphon pipe (m)	Downstream tank (m)	Valve (m)
0.03	0.006	0.09	0.003

2.2.5   Boundary and Initial Conditions

The top surface for both cylindrical tanks is open to the atmosphere, and the siphon pipe is initially primed (e.g., filled with sta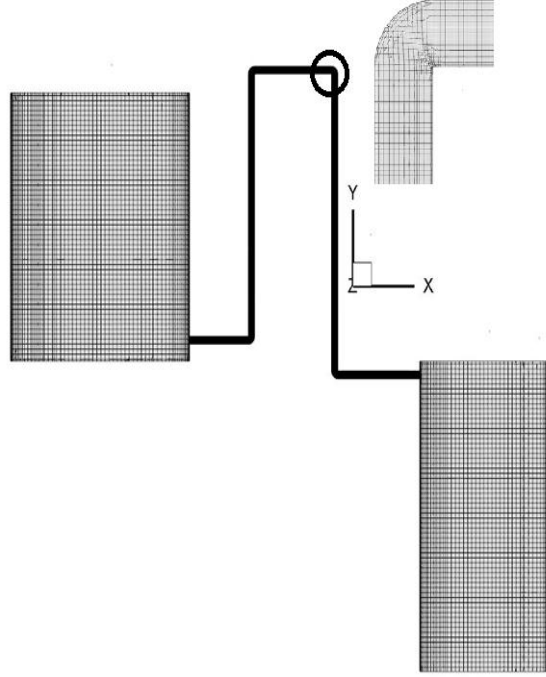gnant water). Non-slip wall boundary condition is imposed at the confining walls of the pipe. The valve is fully closed at $t=0$ and then opened to the desired position. In the numerical model, pressure outlet boundaries with atmospheric pressure are imposed at the top surface of both tanks.

2.2.6   Grid Convergence

An important aspect of using CFD modeling is estimating the contribution of discretization errors. In order to assess the discretization error, the Grid Convergence Index (GCI) was used. This method was proposed by Roache (1997) as a method for reporting discretization errors. The first step of the GCI method is to define grid sizes. For 3D calculations, a representative grid size h can be estimated as:

$$h = \left[\frac{1}{N} \sum_{i=1}^{N} (\Delta V_i) \right]^{1/3} \qquad (2.7)$$

Where ΔV_i is the volume of the ith cell, and N is the total number of cells.

After defining the representative cell sizes, three different grid resolutions are required to run three simulations in order to determine the key variables (ϕ) (e.g., cross-sectional

averaged pressure or velocity profile). The three grid representative cell sizes are h_1, h_2, and h_3 in which h_1 represents the finest mesh and h_3 represents the coarsest mesh.

In this study, ϕ is selected to be the the cross-sectional averaged pressure and velocity profile at three different locations (pipe inlet, top of siphon, and pipe outlet).

The next step is to define mesh refinement ratios, where $r_{21} = h_2/h_1$, and $r_{32} = h_3/h_2$

The apparent order, p, can be calculated using

$$p = \frac{1}{ln(r_{21})} \left| ln \left| \frac{\varepsilon_{32}}{\varepsilon_{21}} \right| + q(p) \right| \tag{2.8}$$

$$q(p) = ln(\frac{r_{21}^2 - s}{r_{32}^2 - s}) \tag{2.9}$$

$$s = 1.sign(\frac{\epsilon_{32}}{\epsilon_{21}}) \tag{2.10}$$

where $\varepsilon_{32} = \phi_3 - \phi_2$, $\varepsilon_{21} = \phi_2 - \phi_1$ with ϕ_k denoting the solution on the kth grid.

The next step involves calculating the extrapolated value

$$\phi_{ext}^{21} = \frac{(r_{21}^p \phi_1 - \phi_2)}{r_{21}^p - 1} \tag{2.11}$$

The final step involves the calculations of approximate relative errors and GCI, which is given by:

$$\phi_{ext}^{21} = \frac{(r_{21}^p \phi_1 - \phi_2)}{r_{21}^p - 1} \tag{2.12}$$

$$e_a^{21} = \left| \frac{\phi_1 - \phi_2}{\phi_1} \right| \tag{2.13}$$

$$GCI_{fine}^{21} = \frac{1.25 e_a^{21}}{r_{21}^p - 1} \tag{2.14}$$

where ϕ_{21}^{ext} is the approximate relative error; e_a^{21} is extrapolated relative error; and GCI_{fine}^{21} is the fine-grid convergence index.

Table 2.2 illustrates the calculation procedure for three selected grids at the pipe inlet. The variables analyzed are the velocity profile and the cross-sectional averaged pressure. According to Table 2.2, the numerical uncertainty in the fine-grid solution for the velocity is 0.058%. It is important to note that this, however, does not account for modeling error.

Table 2.2: Sample calculations of discretization error

	ϕ= Maximum velocity at 2 s	ϕ= Average pressure at 2 s
h_1, h_2, h_3 (m)	0.004, 0.008, 0.01	0.004, 0.008, 0.01
r_{21}	2	2
r_{23}	1.25	1.25
ϕ_1, ϕ_2, ϕ_3	1.728, 1.720, 1.763	9.359, 9.358, 9.361
p	2.714	0.006
ϕ_{ext}^{21}	1.7360	9.30
e_a^{21}	0.046%	0.00106 %
e_{ext}^{21}	0.046%	0.00106%
GCI_{fine}^{21}	0.058%	0.00133%

Figures 2.10 and 2.11 show the centerline velocity profile along y-axis and cross-sectional averaged pressure at the siphon pipe inlet, respectively. The three sets of grids had 208425, 287504, and 530189 cells, respectively.
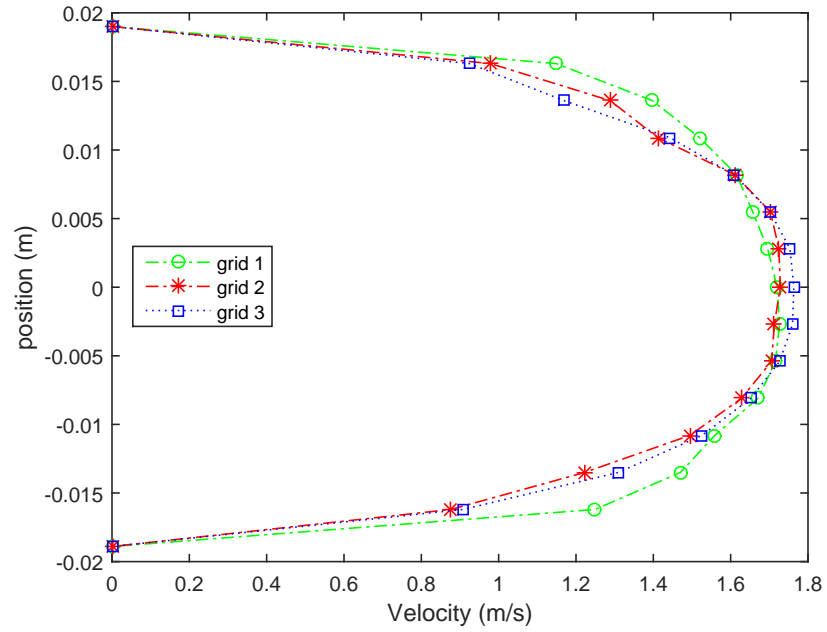
Figure 2.10:   Centerline velocity profile at the siphon inlet, simulation time=2 s
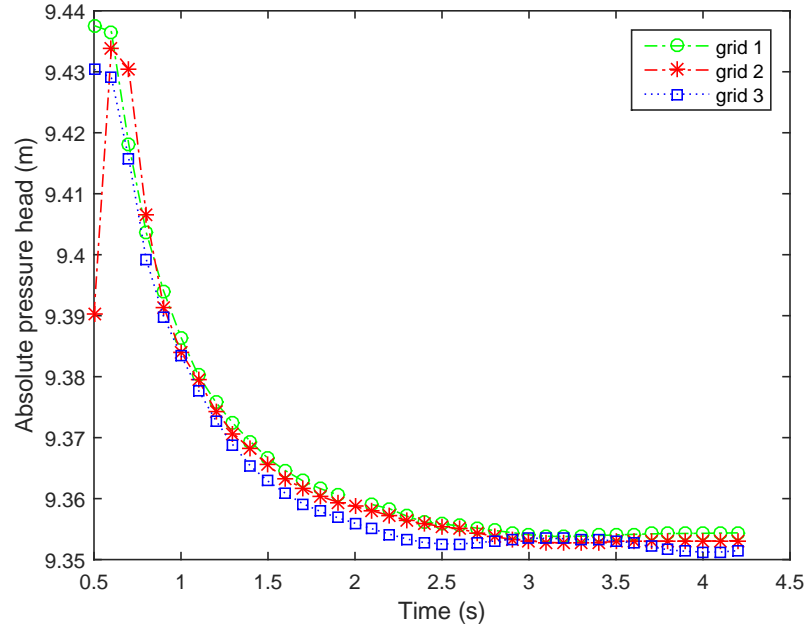
Figure 2.11: Cross-sectional averaged absolute pressure versus time when the valve is fully opened

2.3 Analytical Solution

Siphon flows can be analyzed using the energy equation. Figure 2.12 provides a side view of our experimental siphon pipe.
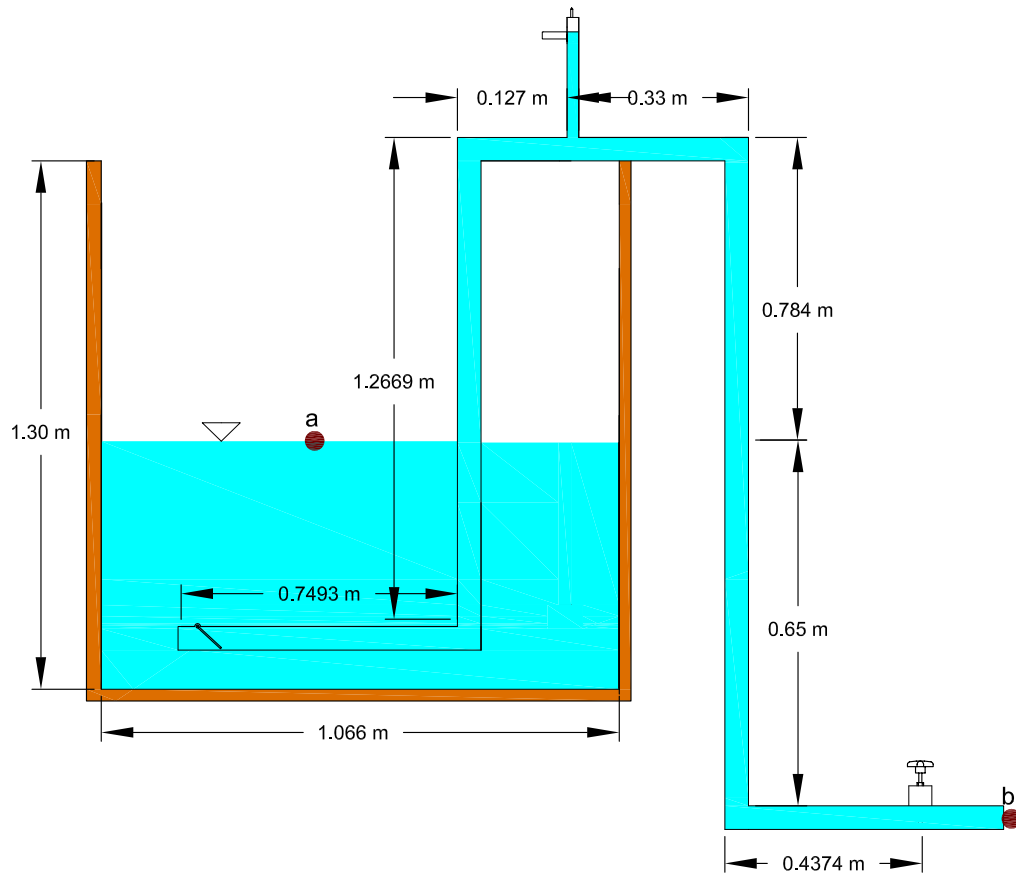
Figure 2.12: Side view of the siphon pipe

The energy equation is given by:

$$Z_a + \frac{P_a}{\gamma} + \frac{V_a^2}{2g} = Z_b + \frac{P_b}{\gamma} + \frac{V_b^2}{2g} + h_f + h_m \qquad (2.15)$$

where, Z_a is the elevation of water in the tank at a pre-specified level, Z_b is the elevation of the pipe centerline at the outlet, P_a is the upstream pressure, P_b is the downstream pressure, V_a is the velocity at point a, V_b is the velocity at point b, γ is the specific weight of water ($9.807\ KN/m^3$), g is the acceleration due to gravity, h_f is the total head loss due to friction, and h_m is the total local head losses.

Because the velocity head at point a is small, eq.(1) can be simplified to:

$$Z_a - Z_b = \frac{V_b^2}{2g} + h_f + h_m \tag{2.16}$$

Thus, the velocity at the outlet can be written as:

$$V = \sqrt{2g(Z_a - Z_b) - (h_f + h_m)} \tag{2.17}$$

To estimate the friction losses, the Darcy-Weisbach formula (Mays, 1996) is used:

$$h_f = \frac{fLV^2}{2gD} \tag{2.18}$$

Where f is a dimensionless friction factor for the pipe, L is the length of the pipe, V is the average flow velocity in the pipe, and D is the diameter of the pipe. The friction factor is function of the Reynolds number and the relative roughness of the pipe. The friction factor f is obtained from the explicit Haaland equation (Haaland, 1983)

$$\frac{1}{\sqrt{f}} = -1.8log_{10}\left[(\frac{\varepsilon/D}{3.7})^{1.11} + \frac{6.9}{R_e}\right] \tag{2.19}$$

Where ε is the roughness height, D is the pipe diameter, R_e is the Reynolds number.

Local head losses h_m are expressed in terms of a loss coefficient multiplied by the velocity head:

$$h_m = \sum k_i(\frac{V^2}{2g}) \tag{2.20}$$

Where k is a dimensionless head loss coefficient for the particular pipe fitting. Typical k values for selected components is shown in Table 2.3.

Table 2.3: Typical k values for selected components within the siphon system (Granger, 1995)

Component	k values
Elbow, Threaded Long Radius 90°	0.7
Entrance Loss	0.5
Check Valve	2
Ball Valve (fully open)	0.05
Ball Valve (75% open)	1.35
Ball Valve (50% open)	27.3
Ball Valve (25% open)	410

Chapter 3: Results

3.1   Experimental Work

A total of 65 tests were conducted. The experimental tests were carried out for three different initial water levels (H) and different valve openings (O). The absolute pressure head versus time is shown in Figures 3.1 through 3.12 for different valve openings. As can be observed in these figures, the pressure in the top of the siphon remains negative (below about 10.3 m) for all valve openings. The pressure at the inlet is higher than that in the outlet for the 100% and 75% valve openings. For the 50% valve opening, the pressure at the inlet is greater than that in the outlet for the first 500 s and then the pressure at the outlet is greater than the inlet. For the 25% valve opening, the outlet pressure is higher than that in the inlet for all times.
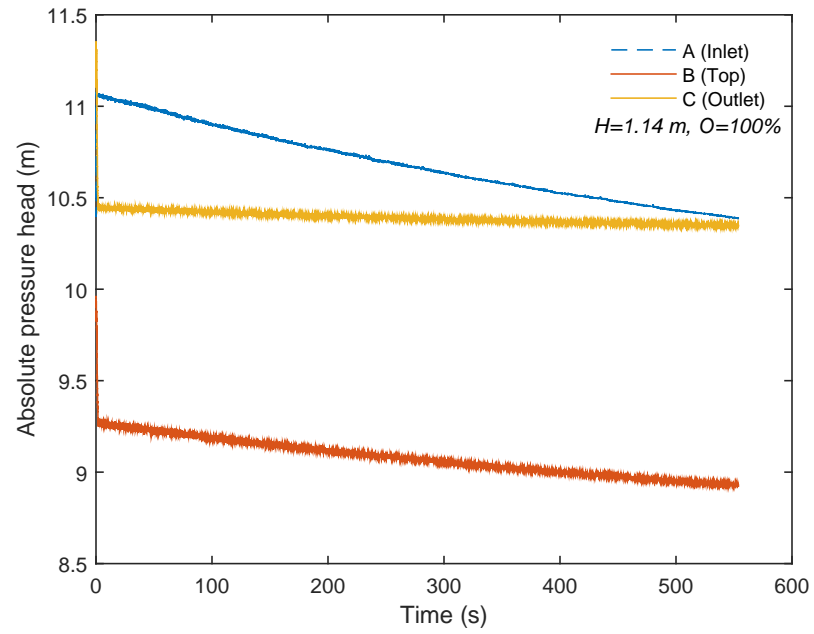
Figure 3.1: Absolute pressure head versus time when the valve is 100% opened
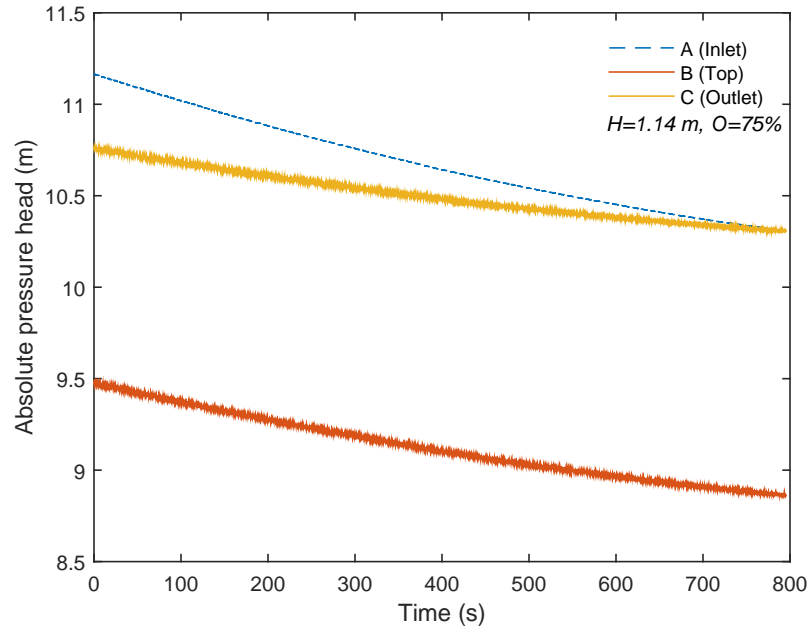
Figure 3.2: Absolute pressure head versus time when the valve is 75% opened
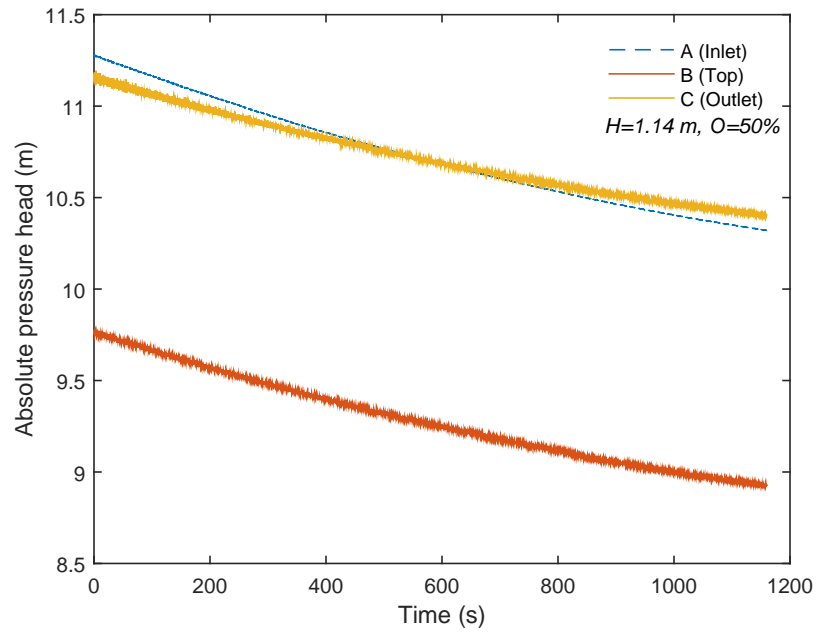
Figure 3.3: Absolute pressure head versus time when the valve is 50% opened
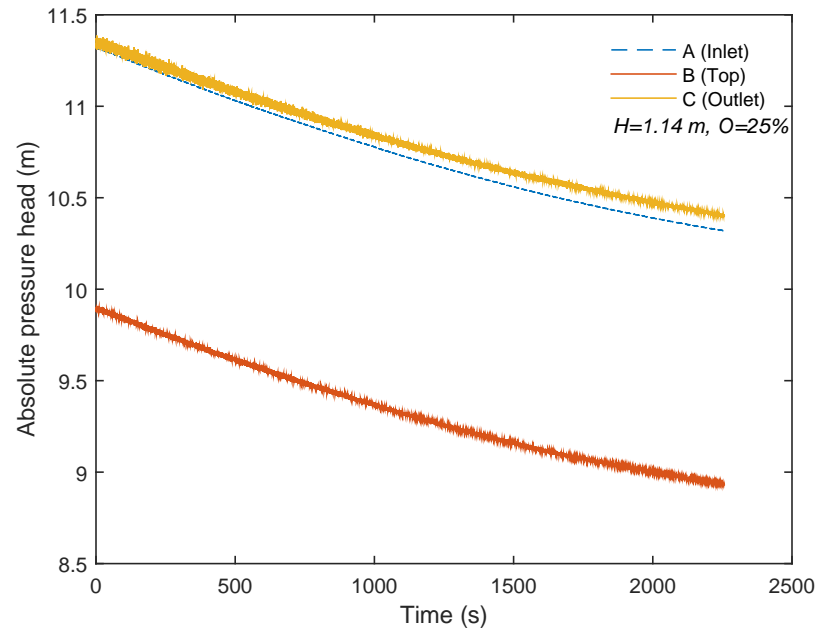
Figure 3.4: Absolute pressure head versus time when the valve is 25% opened
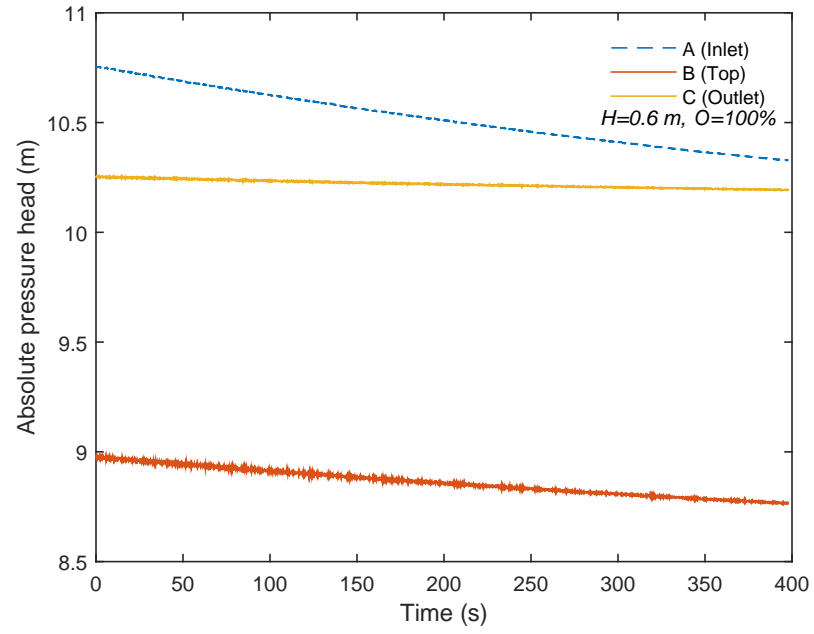
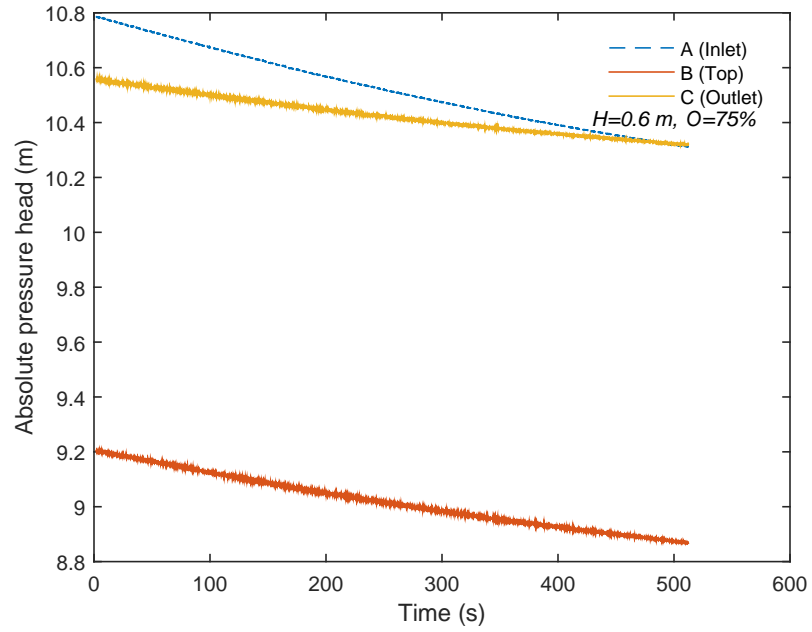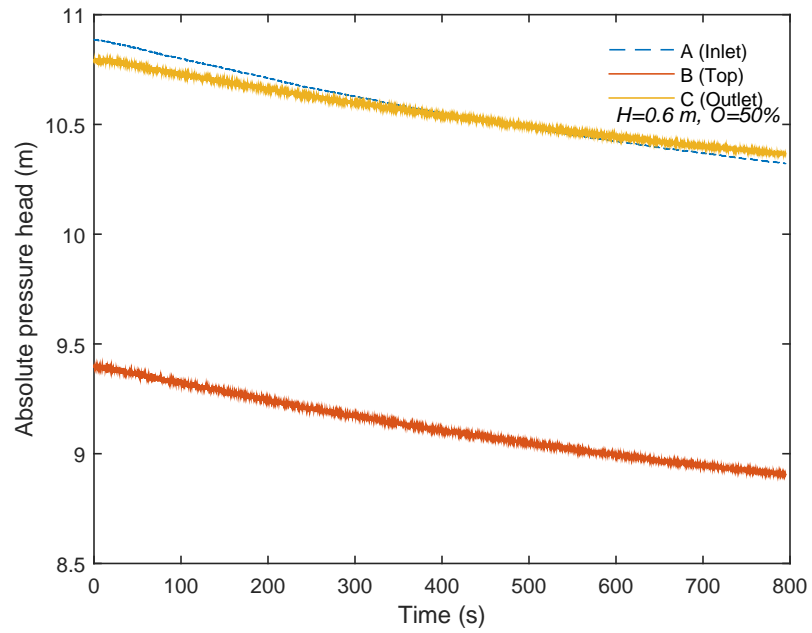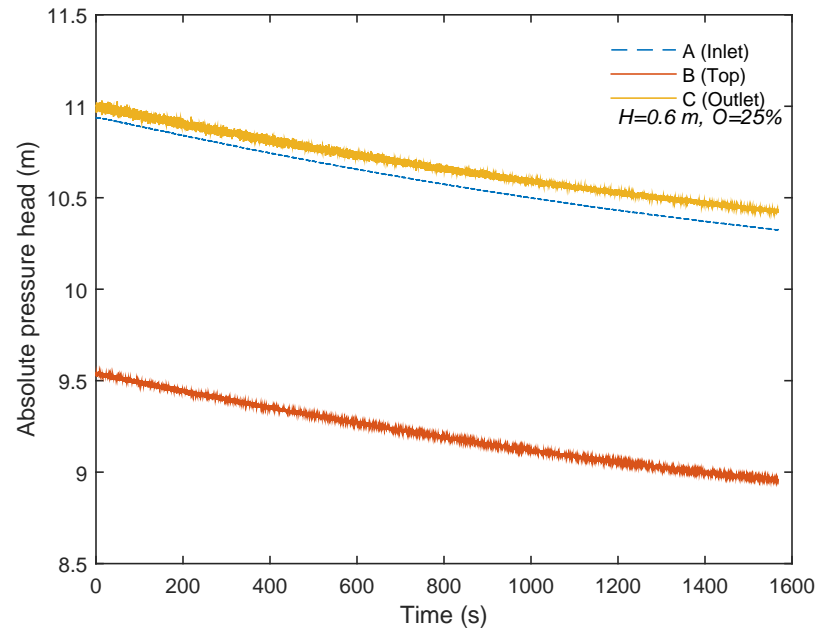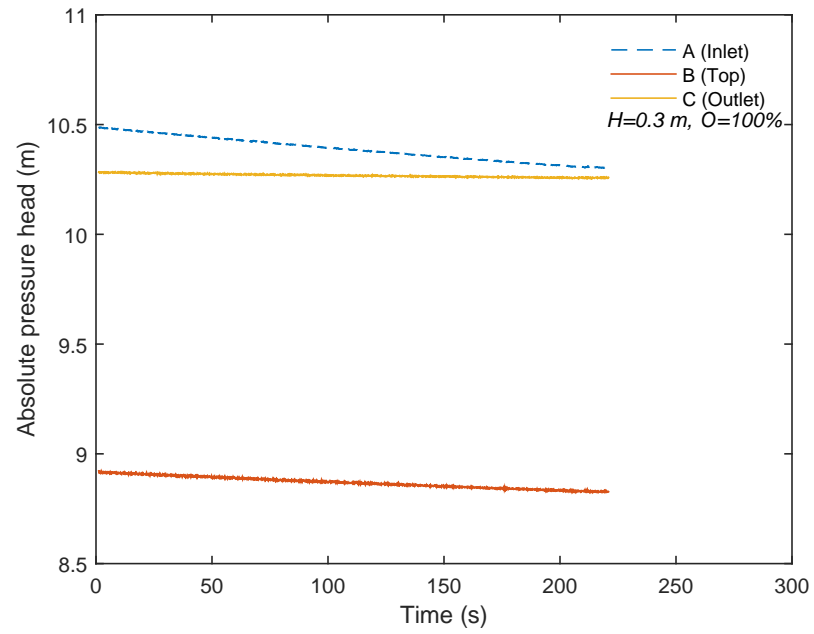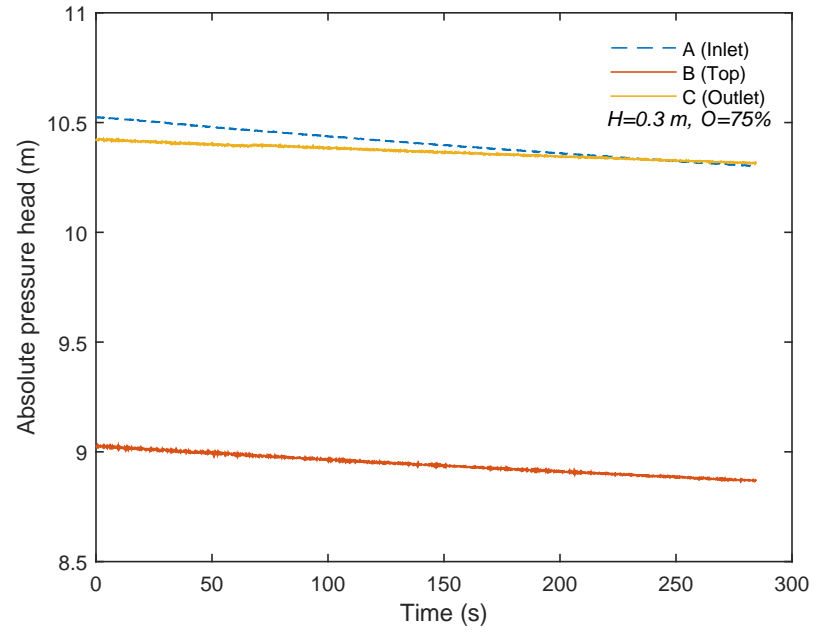Figure 3.5: Absolute pressure head versus time when the valve is 100% opened

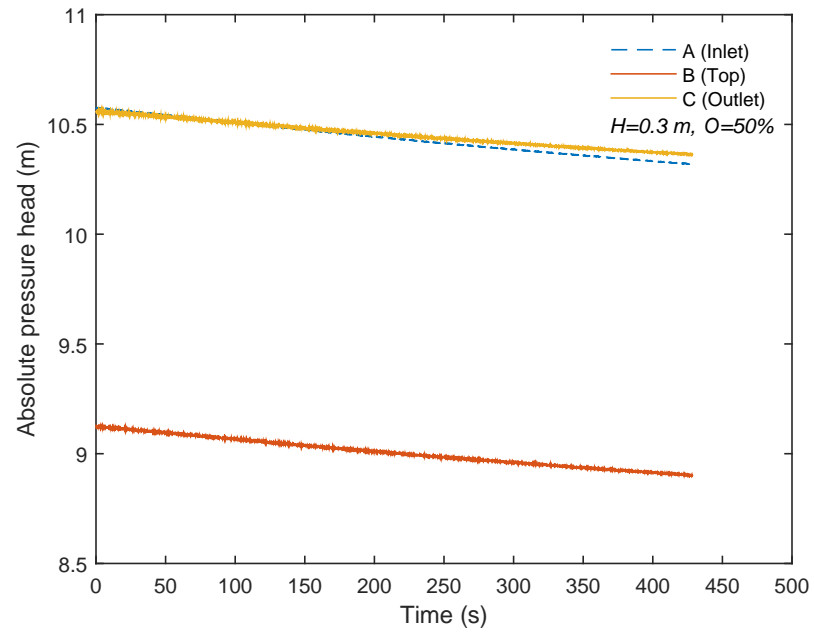Figure 3.6: Absolute pressure head versus time when the valve is 75% opened

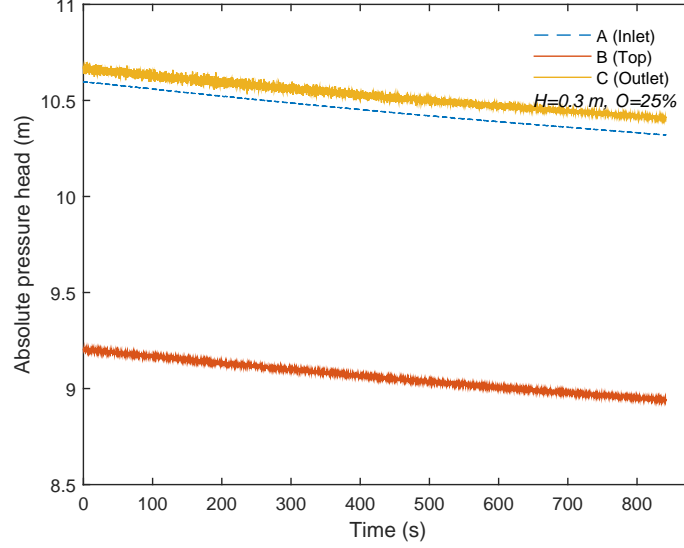Figure 3.7: Absolute pressure head versus time when the valve is 50% opened

Figure 3.8: Absolute pressure head versus time when the valve is 25% opened

Figure 3.9: Absolute pressure head versus time when the valve is 100% opened

Figure 3.10: Absolute pressure head versus time when the valve is 75% opened

Figure 3.11: Absolute pressure head versus time when the valve is 50% opened

Figure 3.12: Absolute pressure head versus time when the valve is 25% opened

3.2 3D Numerical Model

The volume fraction of air and pressure field are shown in Figures   3.13 and   3.14, respectively . Pressure measurements were made at the same location as the laboratory experiments (siphon inlet, top, and outlet). The simulated absolute pressure head traces with different valve openings are shown in Figures   3.15 through   3.26. As can be observed in these figures, the pressure in the top of the siphon remains negative (below about 10.3 m) for all valve openings. For (H=1.14 m), the pressure at the inlet is higher than that in the outlet for the 100%, 75%, 50%, and 25% valve openings. For (H=0.60

m), the pressure at the inlet is higher than that in the outlet for the 100%, 75%, and 50%. However, for the 25% valve opening, the outlet pressure is higher than that in the inlet for all times. For (H= 0.30 m), the pressure at the inlet is higher than that in the outlet for the 100% and 75%. However, for 50% valve openings, the pressure at the inlet is greater than that in the outlet for the first 200 s and then the pressure at the outlet is greater than the inlet, while the outlet pressure is higher than that in the inlet for all times in 25% valve openings. These results are consistent with the experimental results in the second and third initial water levels (H=0.60 m and H=0.3 m).
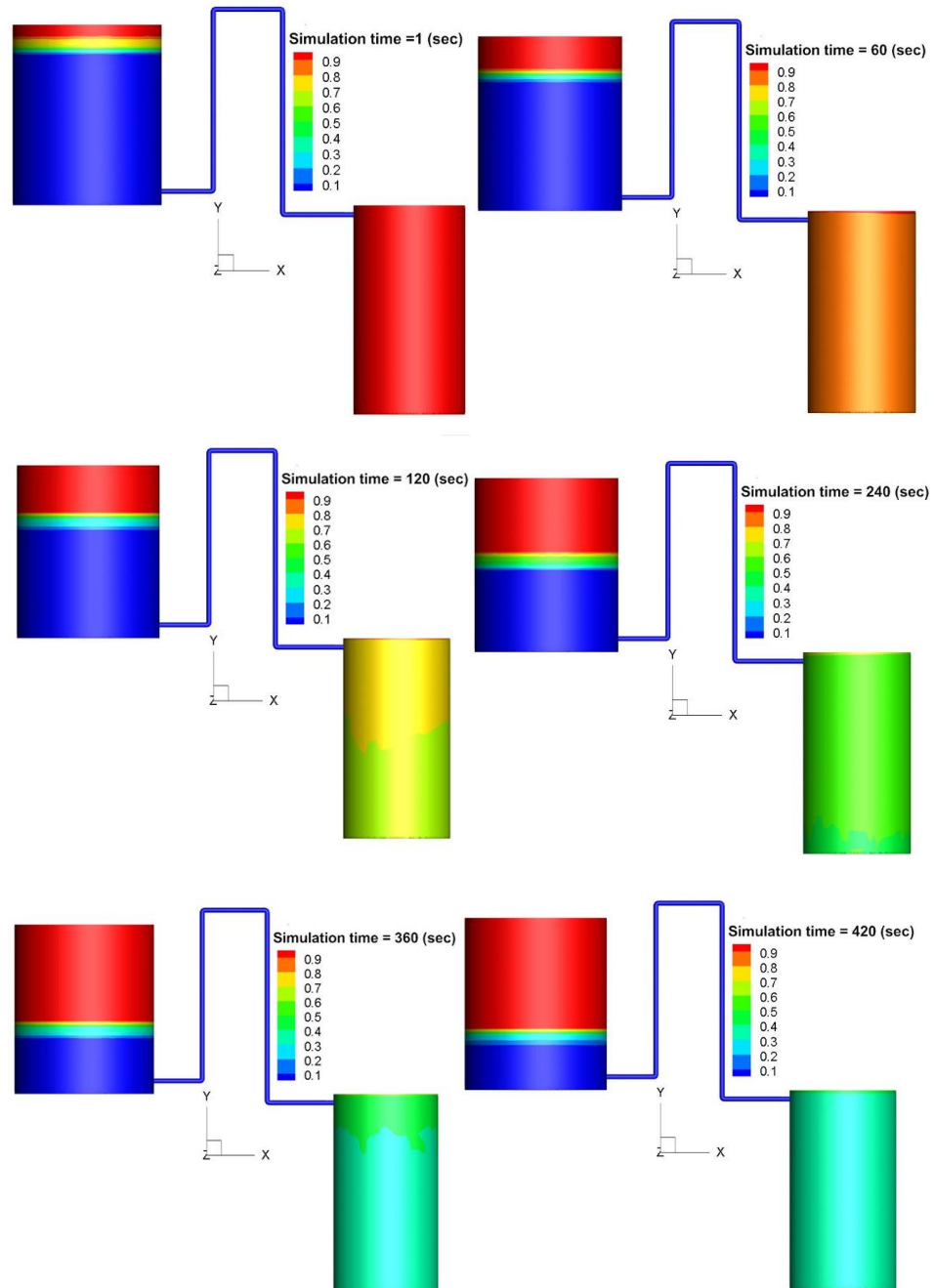
Figure 3.13: Volume fraction of air at various times
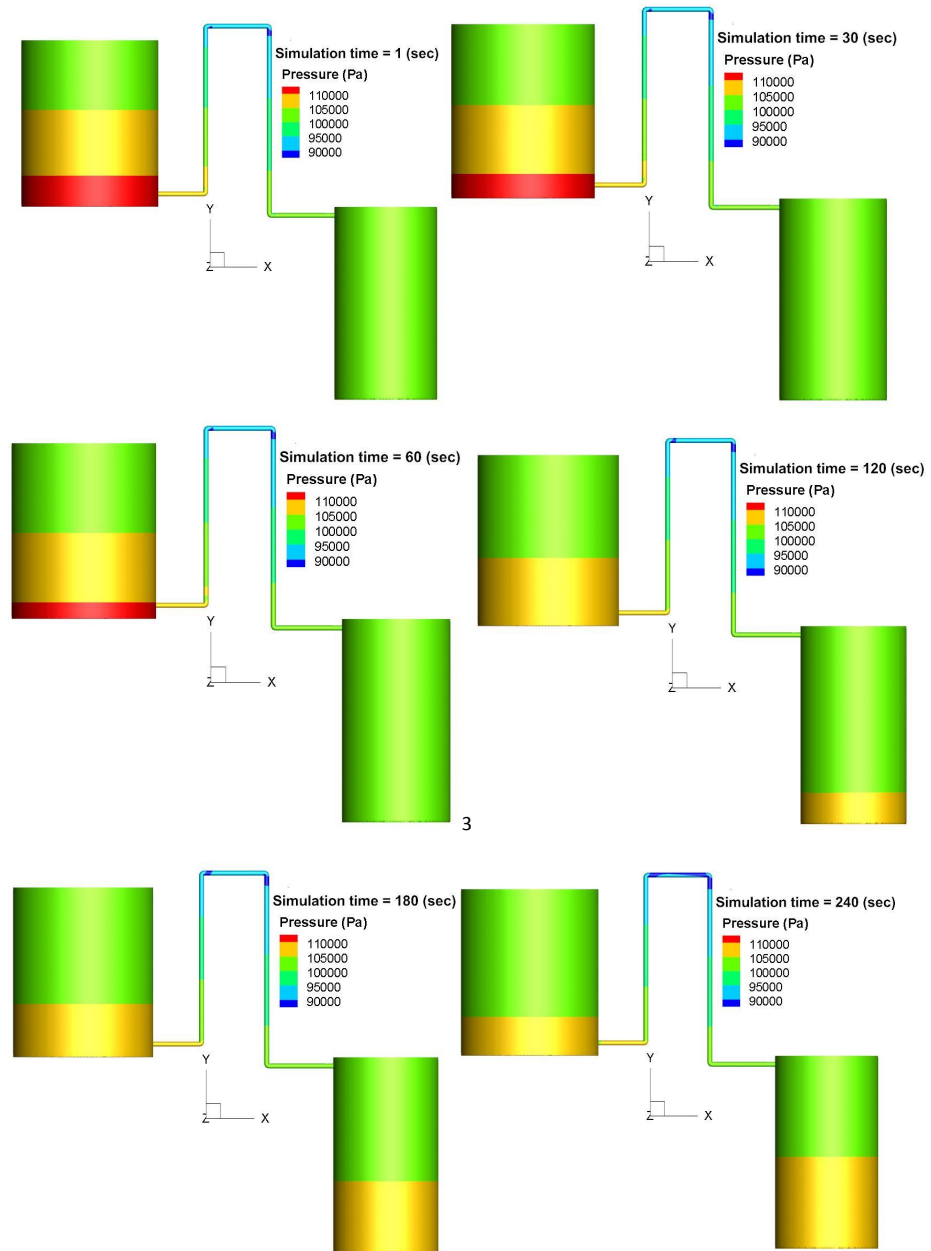
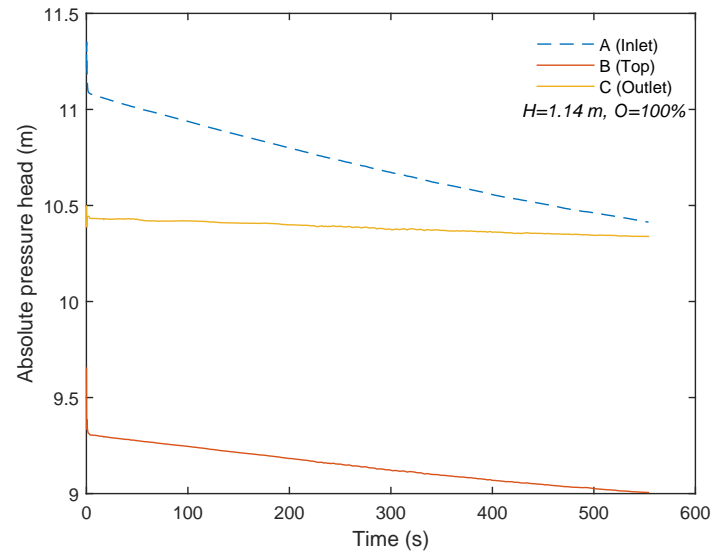Figure 3.14: Absoulate pressure field at various times

Figure 3.15: Absolute pressure head versus time when the valve is 100% opened
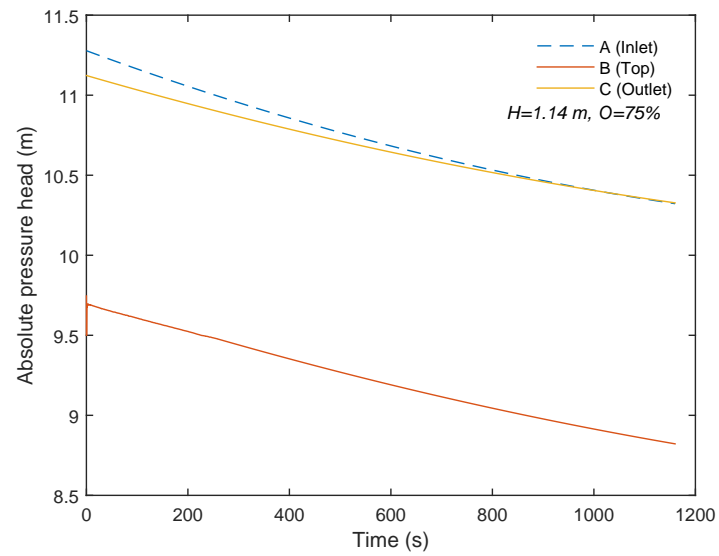

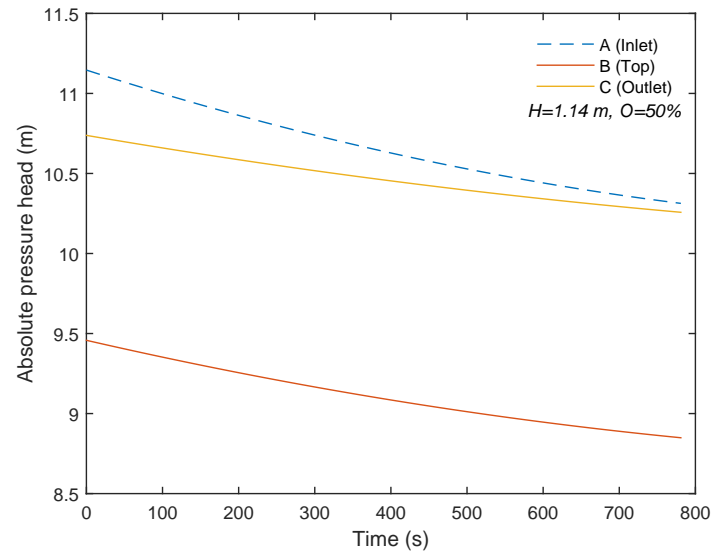Figure 3.16: Absolute pressure head versus time when the valve is 75% opened

Figure 3.17: Absolute pressure head versus time when the valve is 50% opened
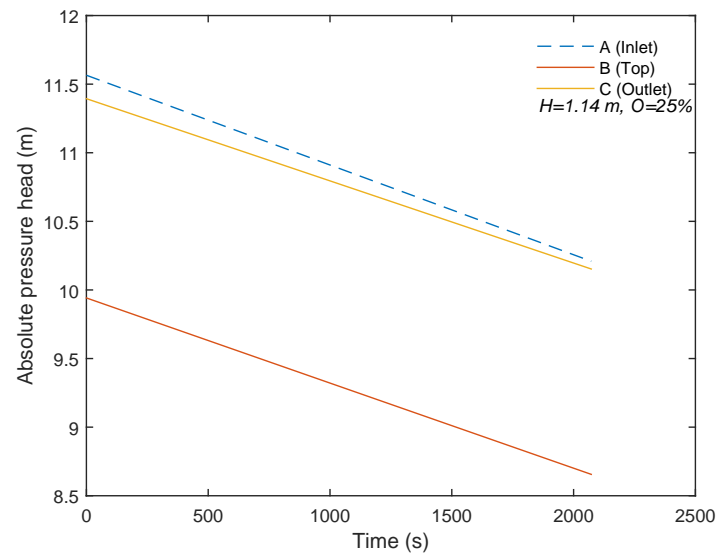

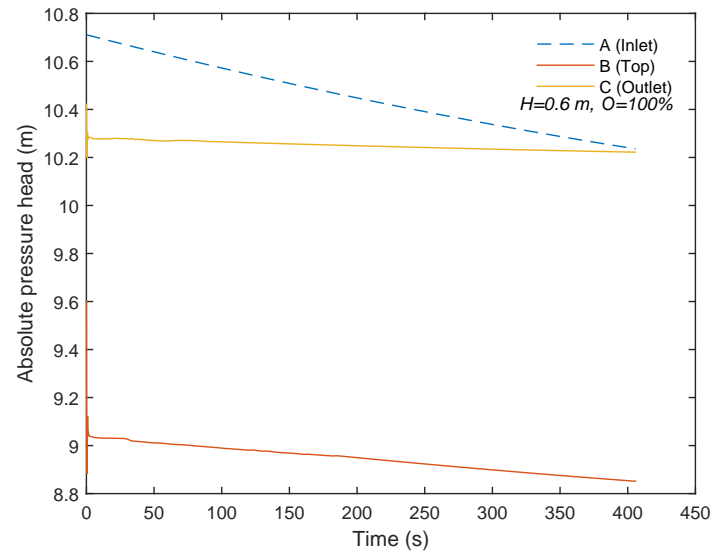Figure 3.18: Absolute pressure head versus time when the valve is 25% opened

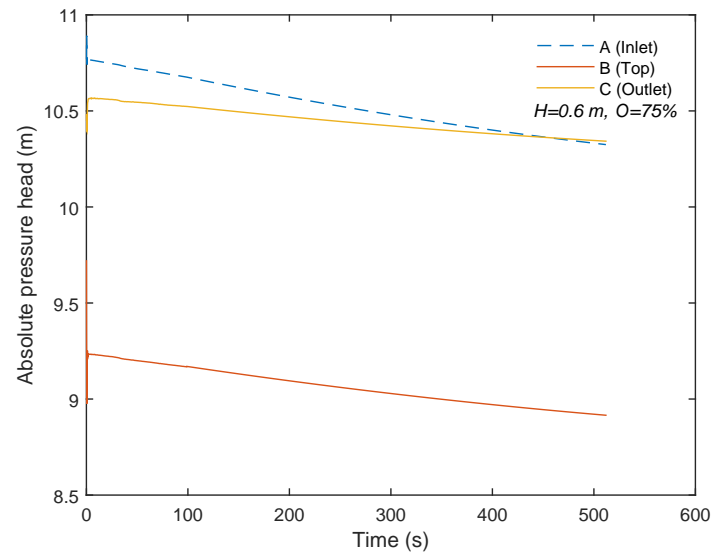Figure 3.19: Absolute pressure head versus time when the valve is 100% opened

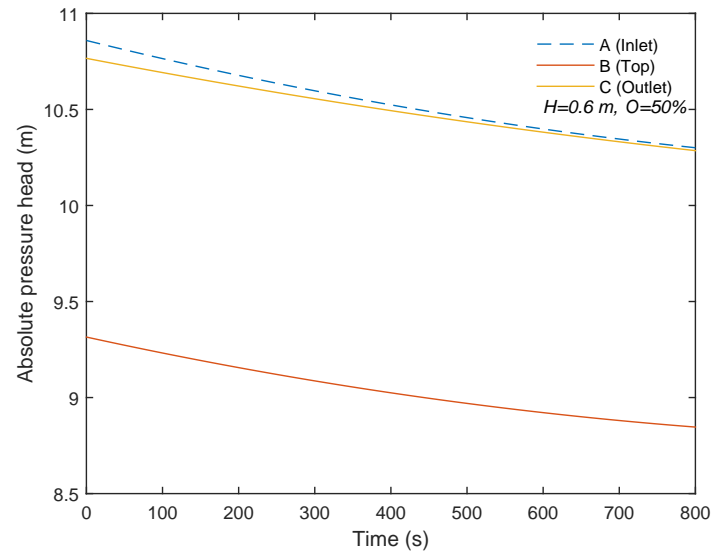Figure 3.20: Absolute pressure head versus time when the valve is 75% opened

Figure 3.21: Absolute pressure head versus time when the valve is 50% opened
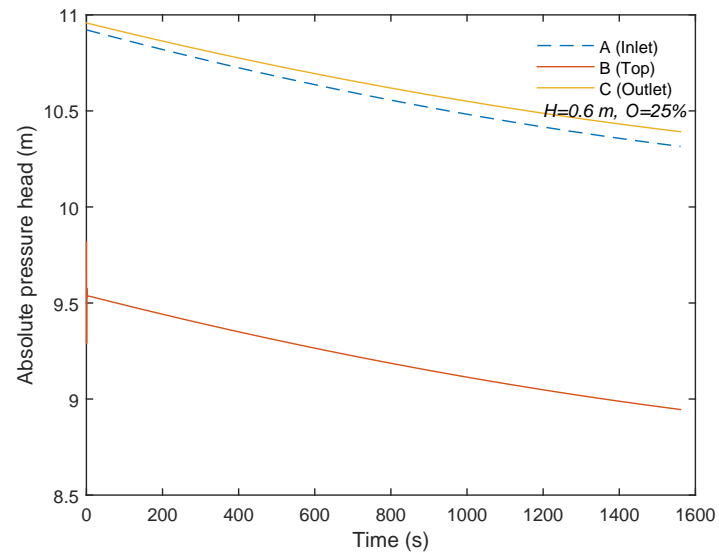

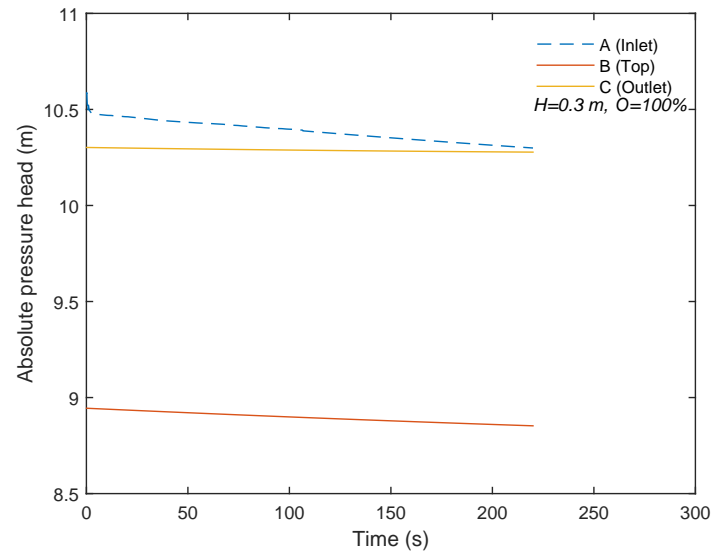Figure 3.22: Absolute pressure head versus time when the valve is 25% opened

Figure 3.23: Absolute pressure head versus time when the valve is 100% opened
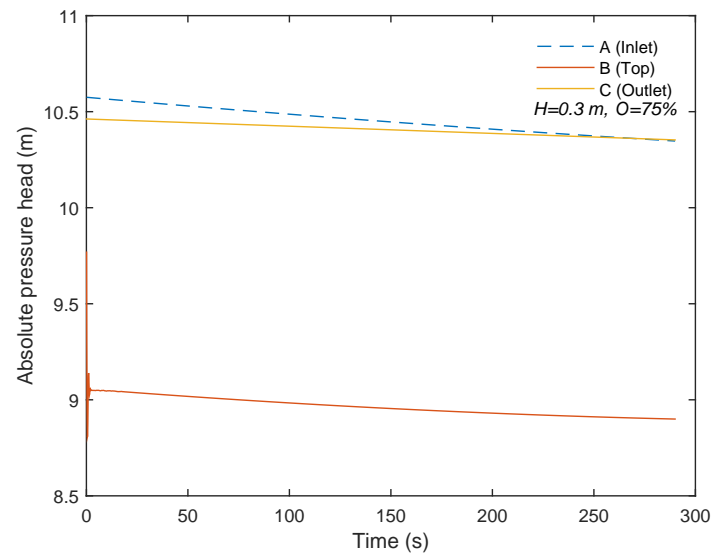

Figure 3.24: Absolute pressure head versus time when the valve is 75% opened
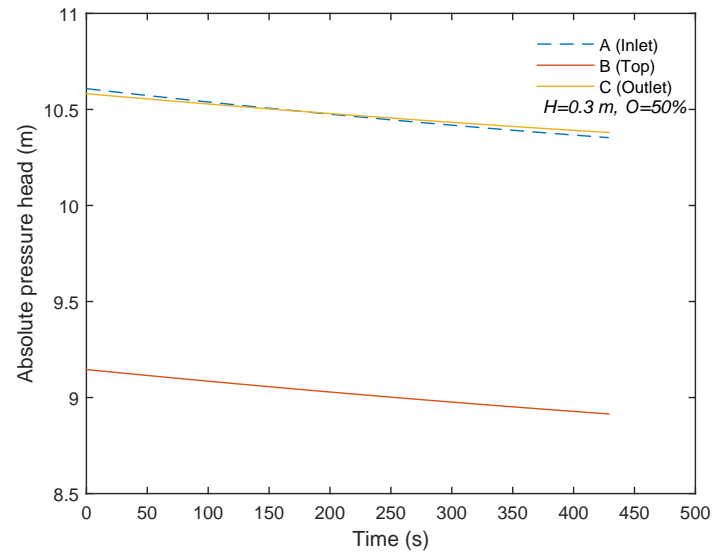
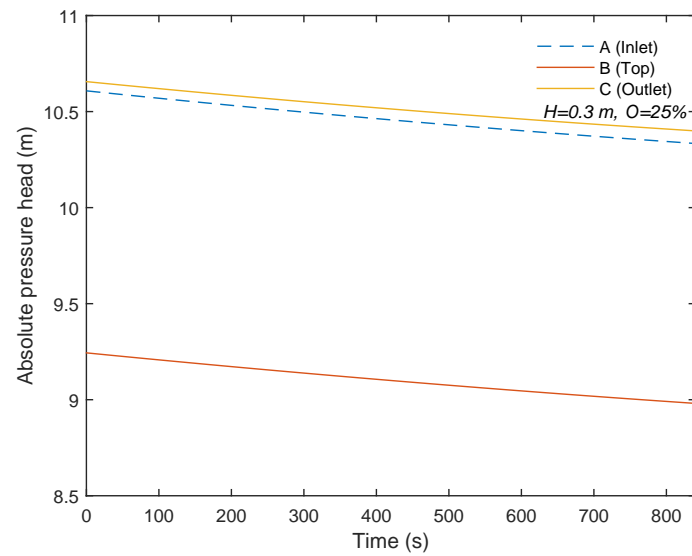Figure 3.25: Absolute pressure head versus time when the valve is 50% opened

Figure 3.26: Absolute pressure head versus time when the valve is 25% opened

3.3 Analytical Solution

The energy equation is applied to determine the absolute pressure head at three loca-
tions within the siphon system (siphon inlet, top, and outlet) for different water initial
conditions and valve openings. The calculated absolute pressure head for different valve
openings are shown in Figures 3.27 through 3.38. As can be observed in these figures,
the pressure in the top of the siphon remains negative (below about 10.3 m) for all valve
openings, which is consistent with the numerical and experimental results. The pressure
at the inlet is higher than that in the outlet for all valve openings. Notice that these
results are different from those of the numerical and experimental ones. The reason is
that the analytical model is one dimensional where the velocity head is constant through-
out the pipe and the analytical model doesn't capture the effects of flow recirculation
or other multi-dimensional flow characteristics. However, as will be shown in the next
section, the analytical results are very similar to those of the numerical and experimental
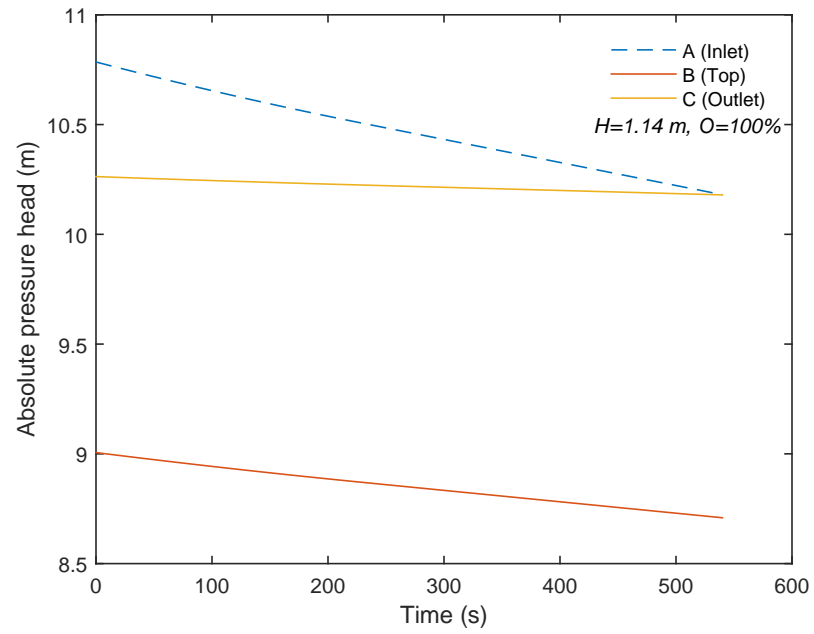results.

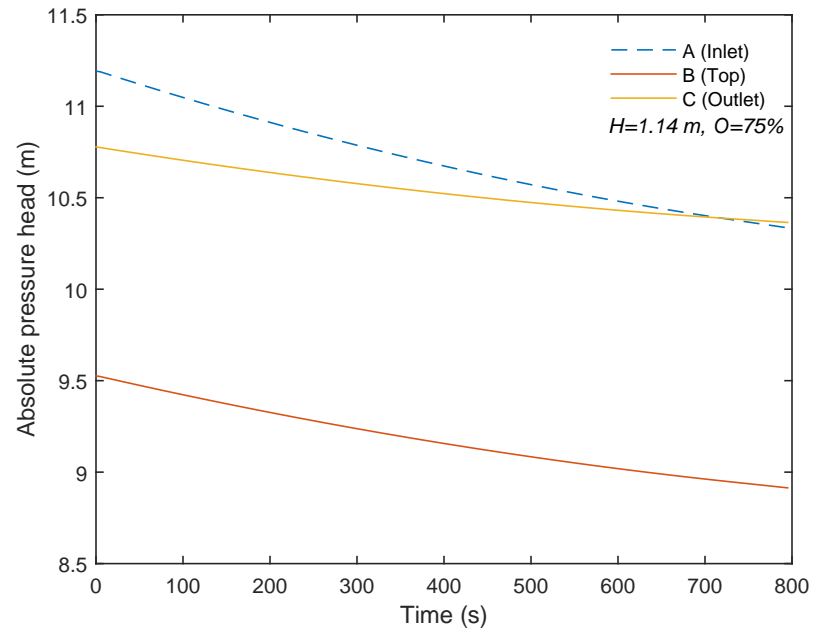Figure 3.27: Absolute pressure head versus time when the valve is 100% opened

Figure 3.28: Absolute pressure head versus time when the valve is 75% opened
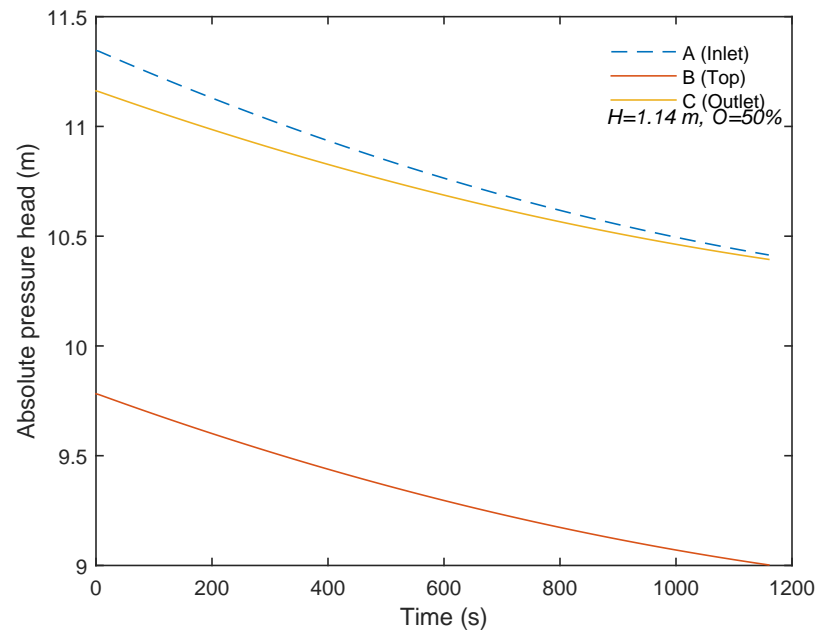

Figure 3.29: Absolute pressure head versus time when the valve is 50% opened
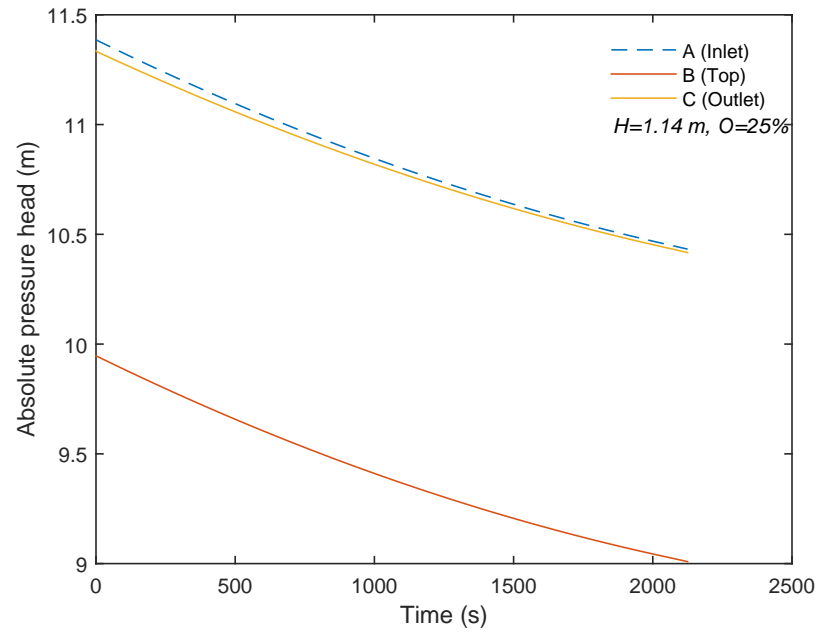
Figure 3.30: Absolute pressure head versus time when the valve is 25% opened

Figure 3.31: Absolute pressure head versus time when the valve is 100% opened

Figure 3.32: Absolute pressure head versus time when the valve is 75% opened

Figure 3.33: Absolute pressure head versus time when the valve is 50% opened

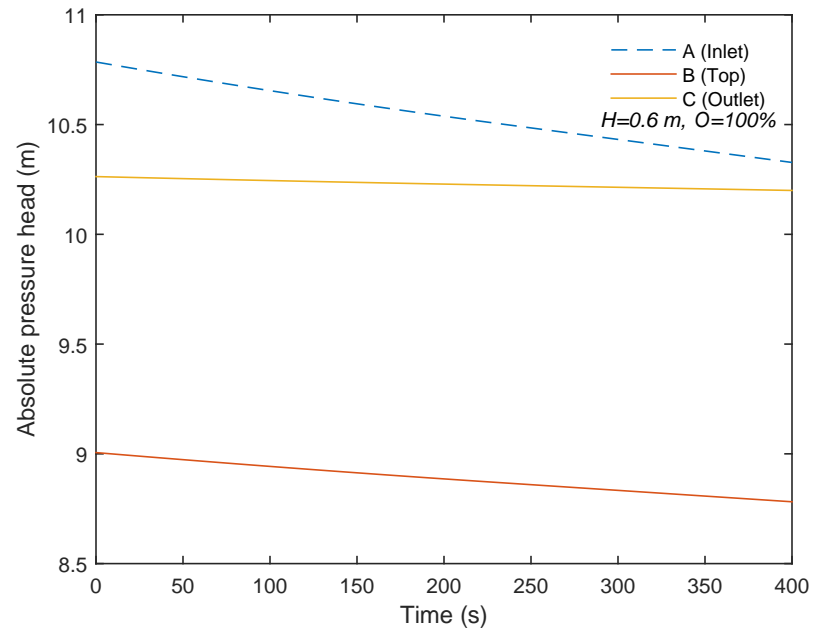Figure 3.34: Absolute pressure head versus time when the valve is 25% opened

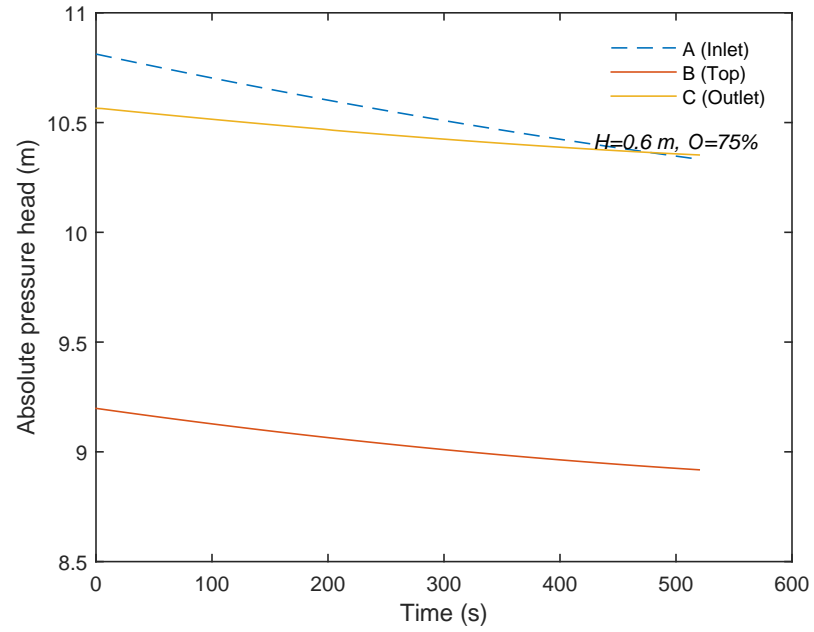Figure 3.35: Absolute pressure head versus time when the valve is 100% opened

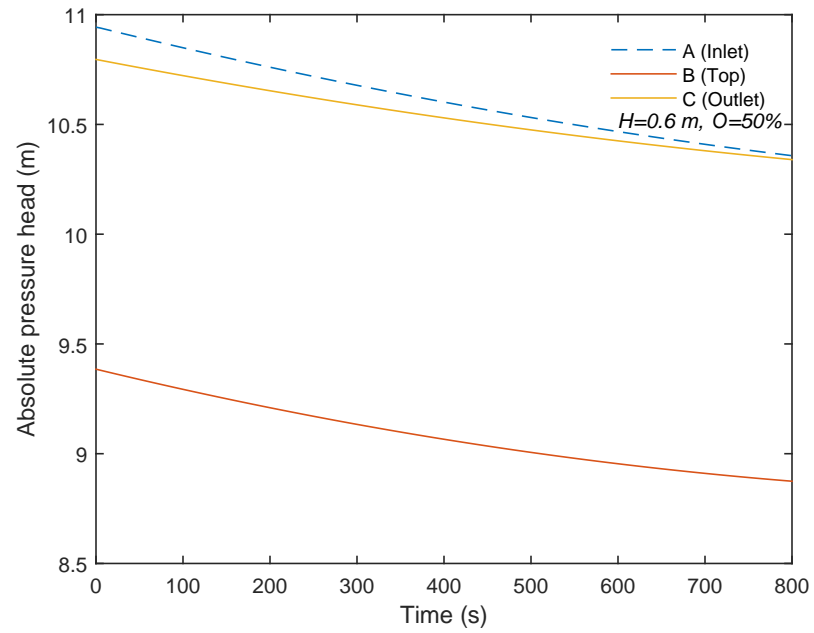Figure 3.36: Absolute pressure head versus time when the valve is75% opened

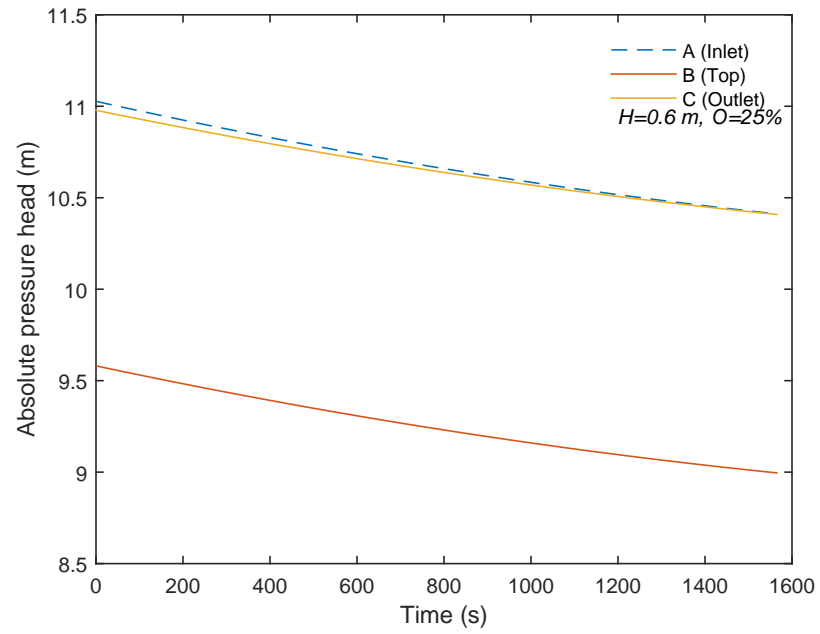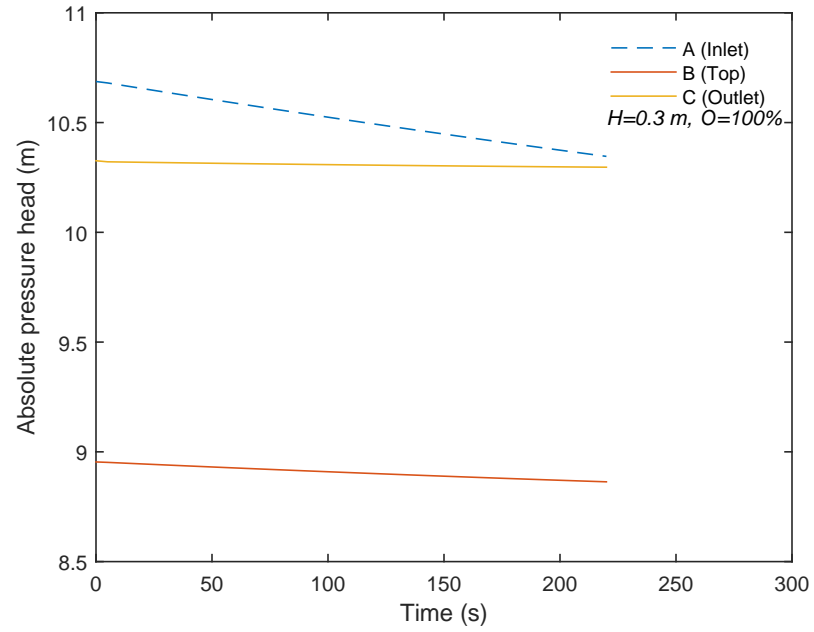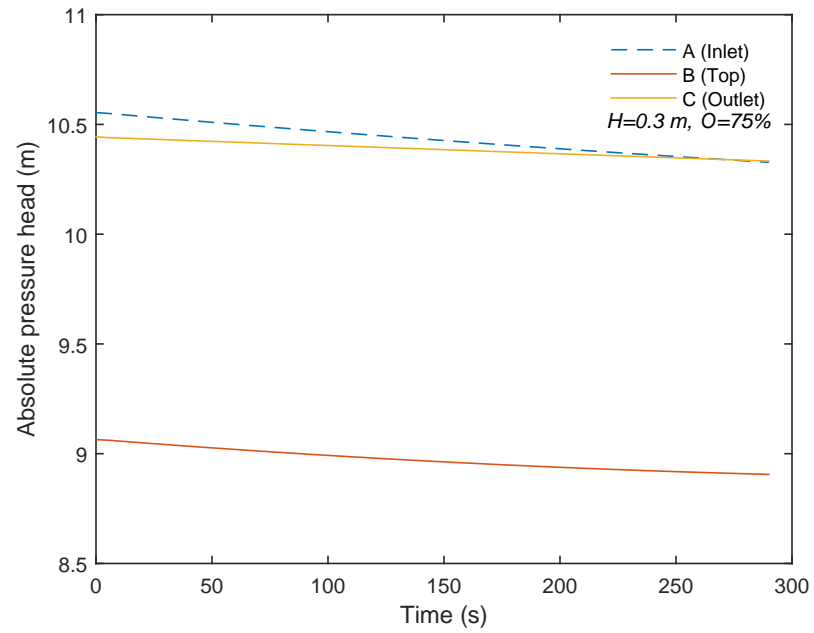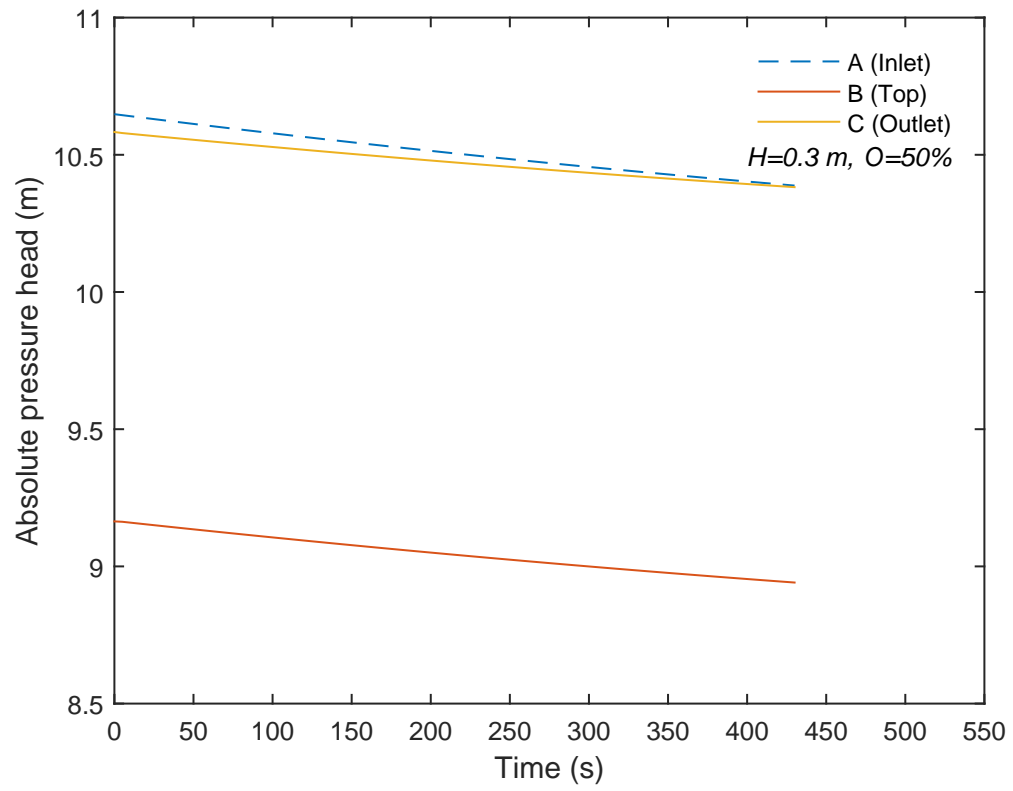Figure 3.37: Absolute pressure head versus time when the valve is 50% opened
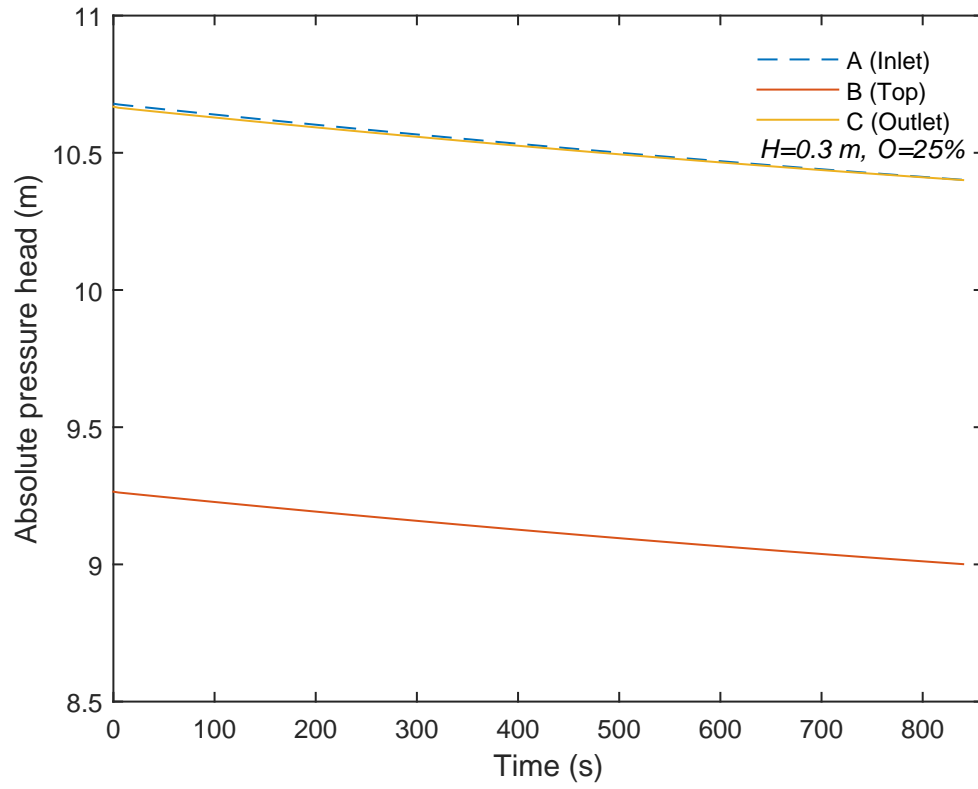
Figure 3.38: Absolute pressure head versus time when the valve is 25% opened

3.4 Comparison of Analytical, Numerical, and Experimental Results

The comparison of analytical, numerical, and experimental absolute pressure head traces with different valve openings are shown in Figures 3.39 through 3.74. As observed in

these figures, the prediction of the draining rate is well captured by the analytical, numerical and experimental results. This means that the operation of the proposed siphon system could be predicted with a simple one-dimensional analytical model.

Figure 3.39: Comparison of Analytical, Numerical, and Experimental absolute pressure head traces at siphon inlet: H=1.14 m O=100%

Figure 3.40: Comparison of Analytical, Numerical, and Experimental absolute pressure head traces at siphon top: H=1.14 m O=100%

Figure 3.41: Comparison of Analytical, Numerical, and Experimental absolute pressure head traces at siphon outlet: H=1.14 m O=100%

Figure 3.42: Comparison of Analytical, Numerical, and Experimental absolute pressure head traces at siphon inlet: H=1.14 m O=75%

Figure 3.43: Comparison of Analytical, Numerical, and Experimental absolute pressure head traces at siphon top: H=1.14 m O=75%

Figure 3.44: Comparison of Analytical, Numerical, and Experimental absolute pressure head traces at siphon outlet: H=1.14 m O=75%
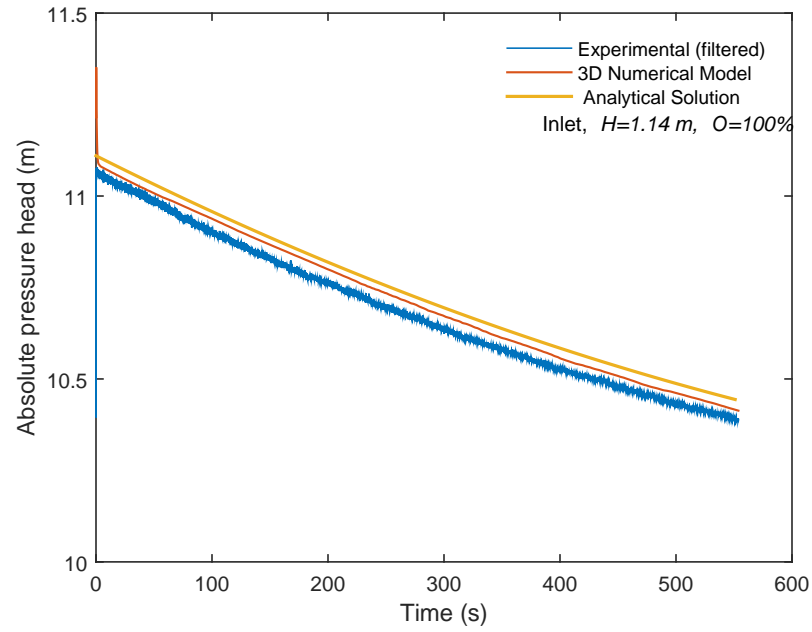
Figure 3.45: Comparison of Analytical, Numerical, and Experimental absolute pressure head traces at siphon inlet: $H{=}1.14$ m $O{=}50\%$
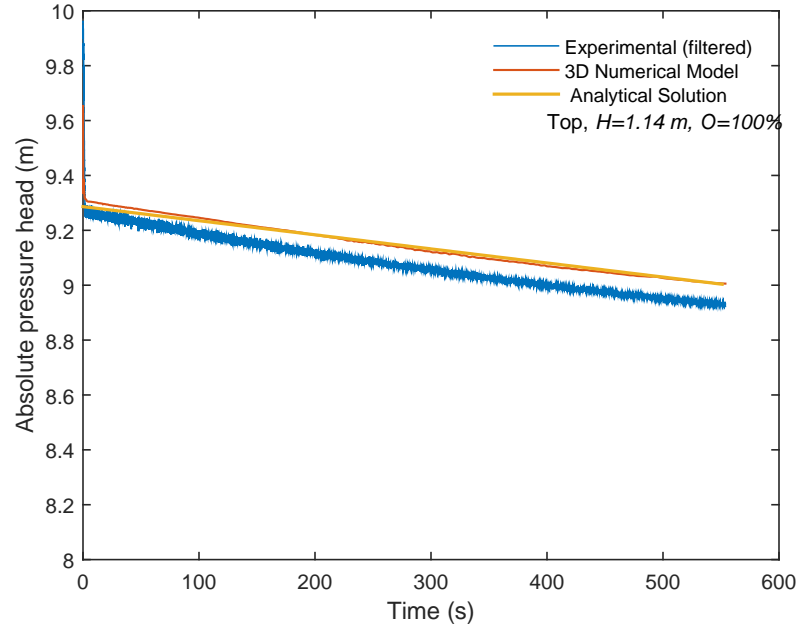
Figure 3.46: Comparison of Analytical, Numerical, and Experimental absolute pressure head traces at siphon top:H=1.14 m (O)=50%
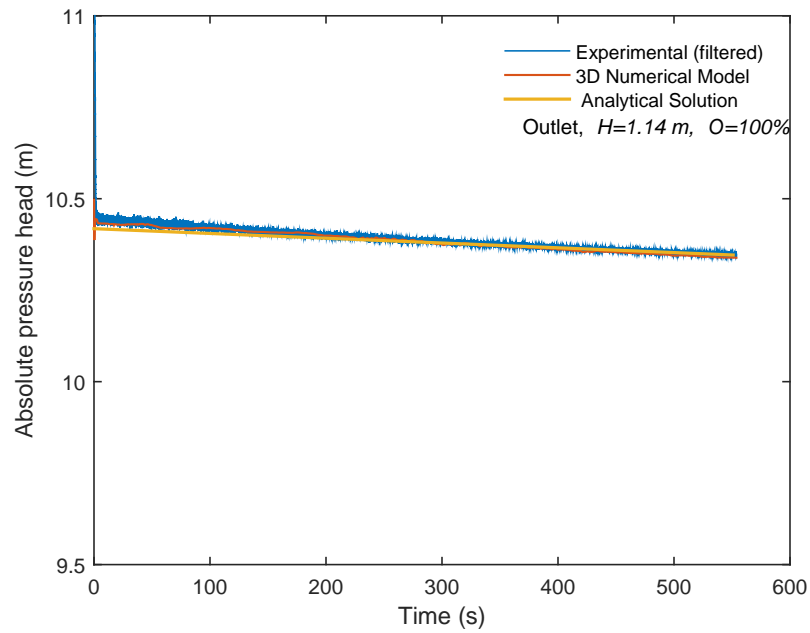

Figure 3.47: Comparison of Analytical, Numerical, and Experimental absolute pressure head traces at siphon outlet: H=1.14 mO=50%
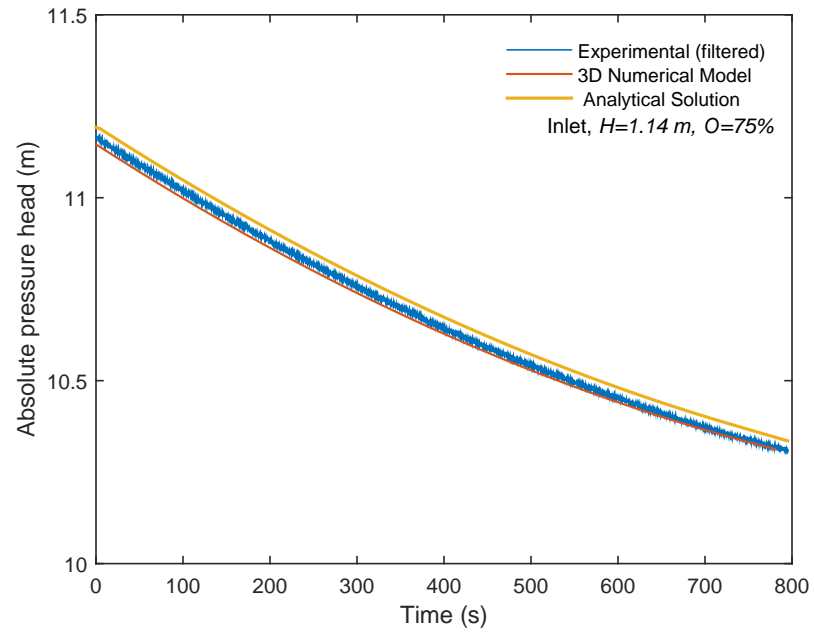
Figure 3.48: Comparison of Analytical, Numerical, and Experimental absolute pressure head traces at siphon inlet: H=1.14 m O=25%
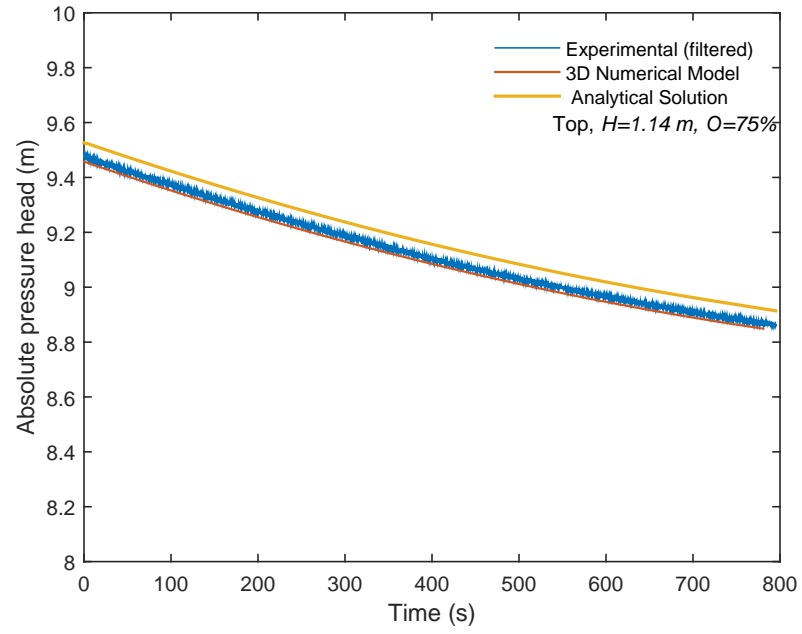
Figure 3.49: Comparison of Analytical, Numerical, and Experimental absolute pressure head traces at siphon top: H=1.14 m O=25%
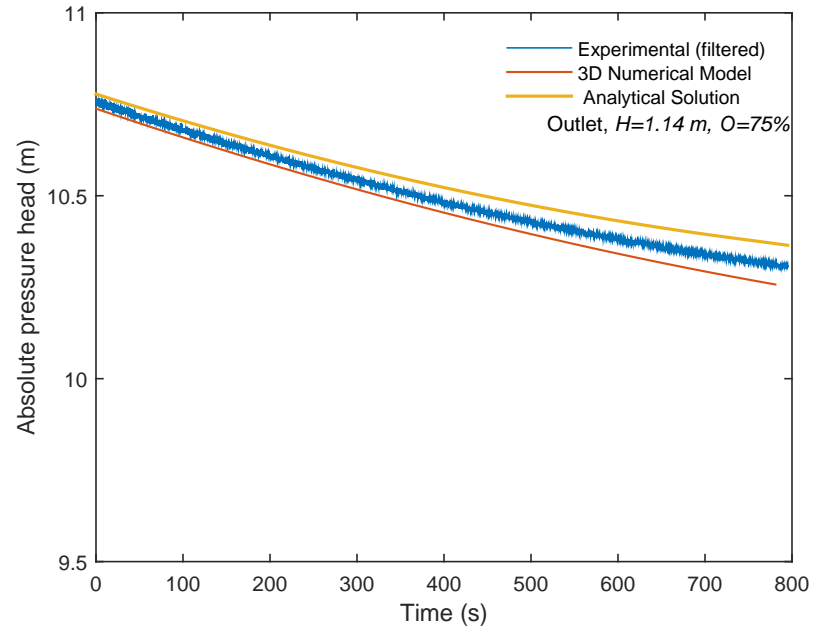

Figure 3.50: Comparison of Analytical, Numerical, and Experimental absolute pressure head traces at siphon outlet: H=1.14 m O=25%
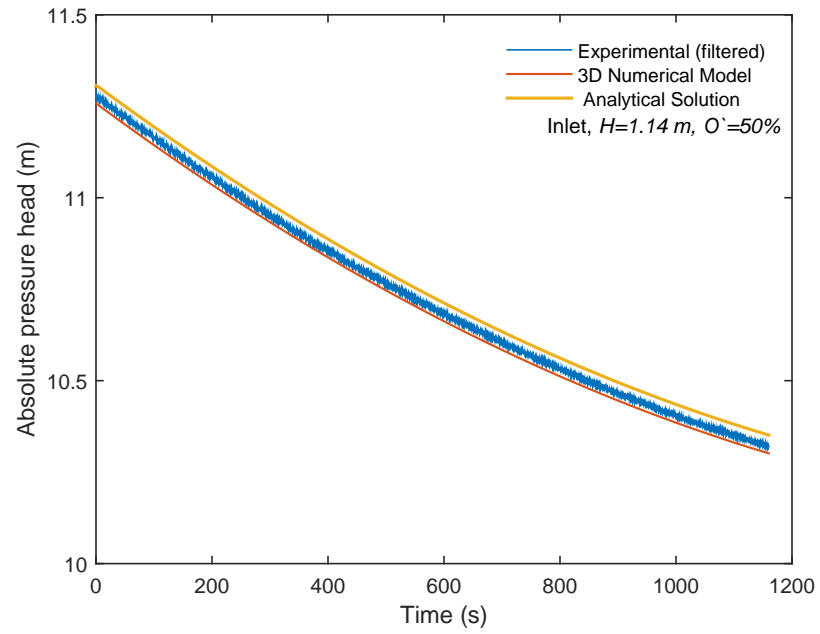
Figure 3.51: Comparison of Analytical, Numerical, and Experimental absolute pressure head traces at siphon inlet: H=0.6m O=100%

Figure 3.52: Comparison of Analytical, Numerical, and Experimental absolute pressure head traces at siphon top: H=0.6m O=100%

Figure 3.53: Comparison of Analytical, Numerical, and Experimental absolute pressure head traces at siphon outlet: H=0.6m O=100%

Figure 3.54: Comparison of Analytical, Numerical, and Experimental absolute pressure head traces at siphon inlet: H=0.6m O=75%
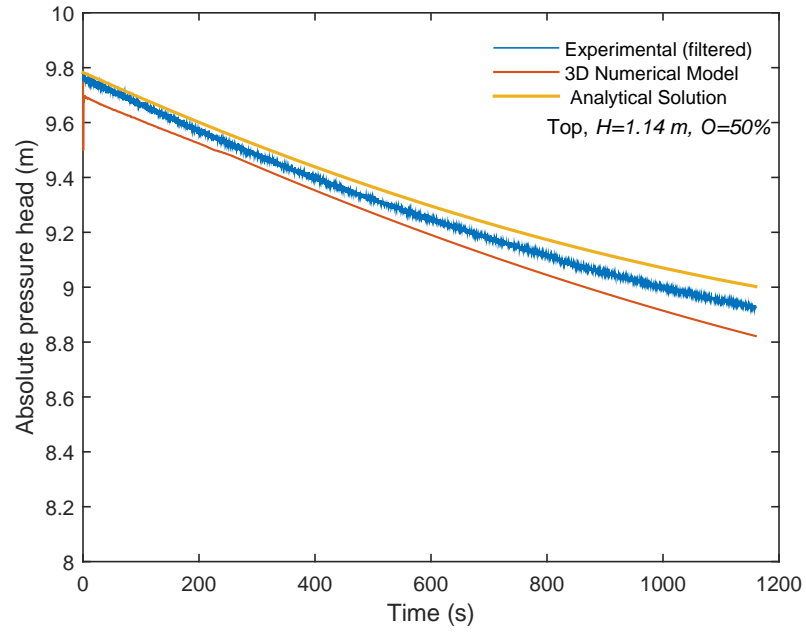
Figure 3.55: Comparison of Analytical, Numerical, and Experimental absolute pressure head traces at siphon top: H=0.6m O=75%

Figure 3.56: Comparison of Analytical, Numerical, and Experimental absolute pressure head traces at siphon outlet: H=0.6m O=75%
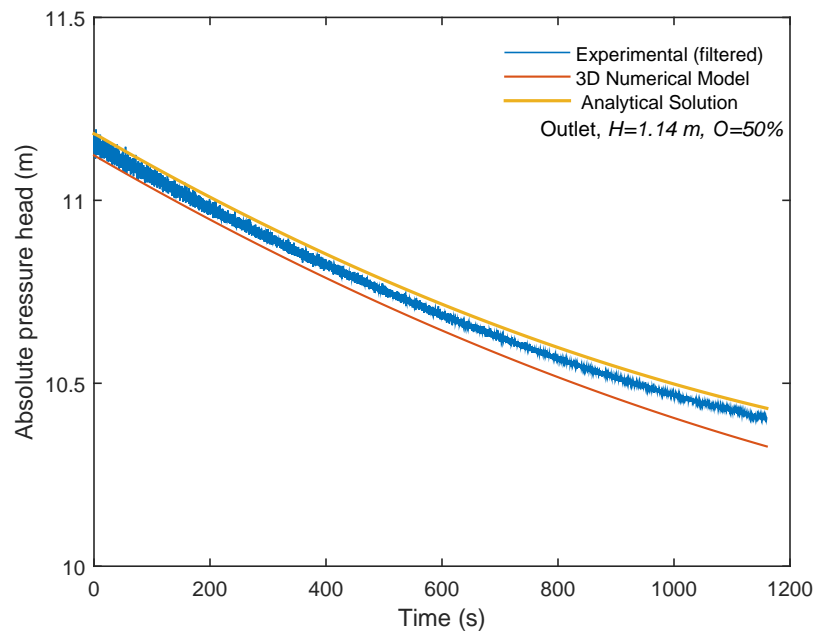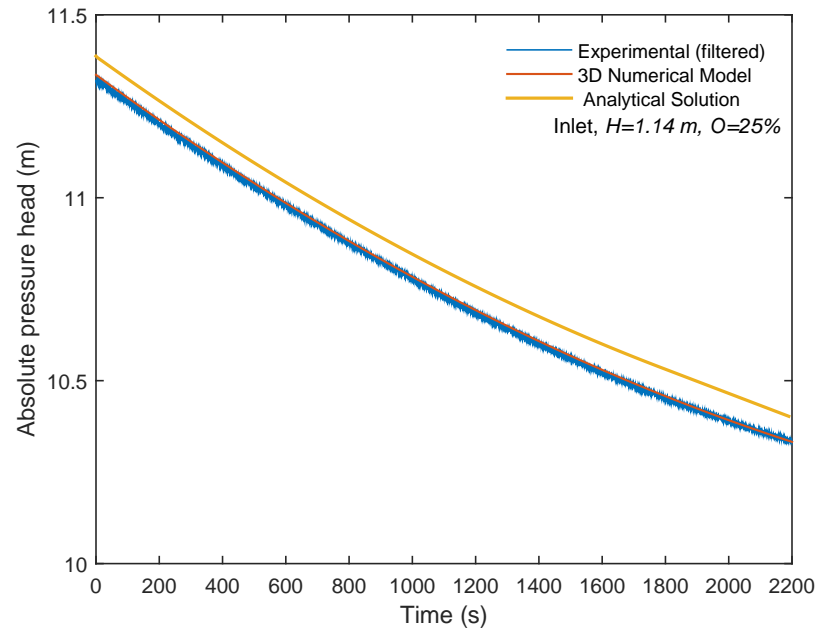
Figure 3.57: Comparison of Analytical, Numerical, and Experimental absolute pressure head traces at siphon inlet: H=0.6m O=50%
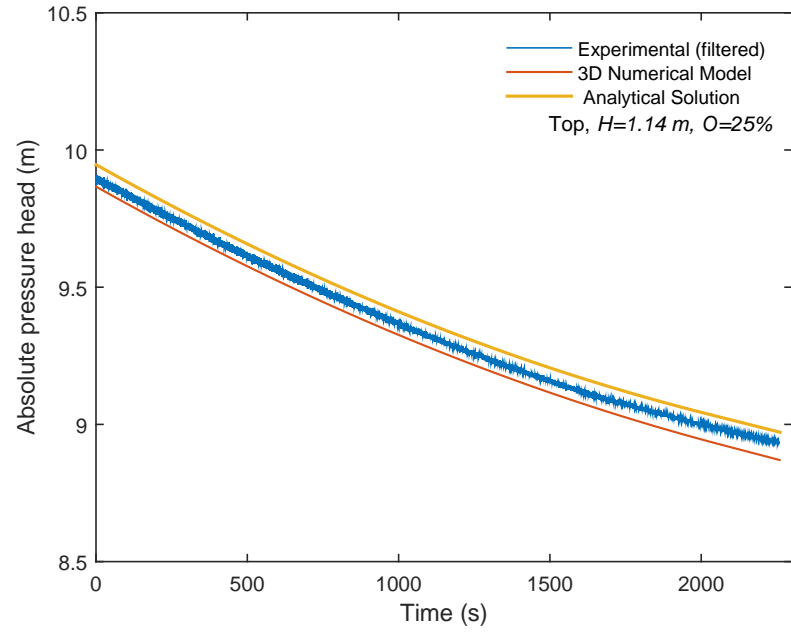

Figure 3.58: Comparison of Analytical, Numerical, and Experimental absolute pressure head traces at siphon top: H=0.6m O=50%
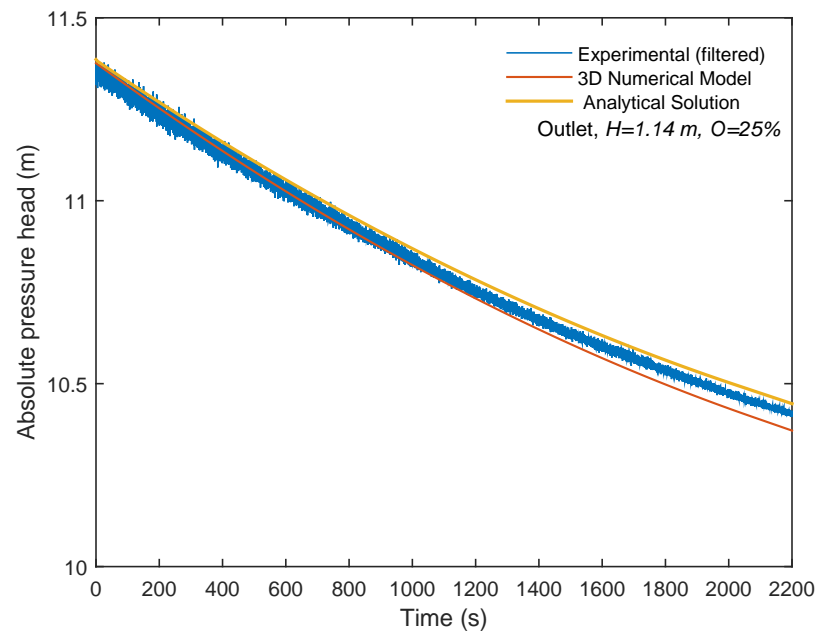
Figure 3.59: Comparison of Analytical, Numerical, and Experimental absolute pressure head traces at siphon outlet: H=0.6m O=50%

Figure 3.60: Comparison of Analytical, Numerical, and Experimental absolute pressure head traces at siphon inlet: H=0.6m O=25%

Figure 3.61: Comparison of Analytical, Numerical, and Experimental absolute pressure head traces at siphon top: H=0.6m O=25%

Figure 3.62: Comparison of Analytical, Numerical, and Experimental absolute pressure head traces at siphon outlet: H=0.6m O=25%
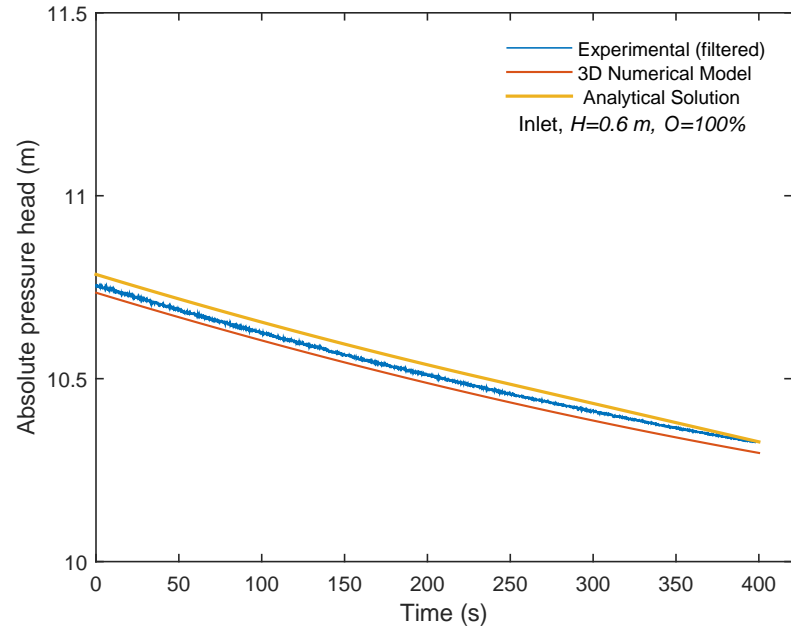
Figure 3.63: Comparison of Analytical, Numerical, and Experimental absolute pressure head traces at siphon inlet: H=0.3m O=100%
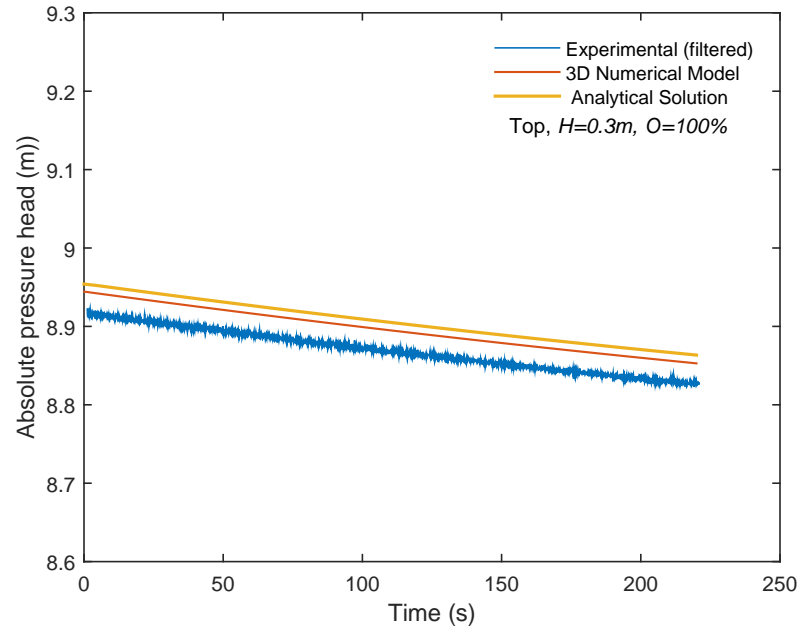
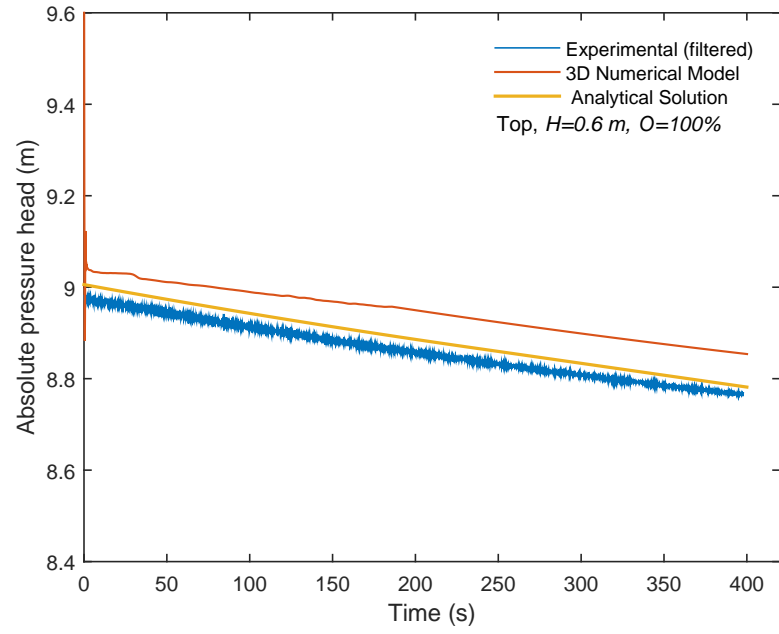Figure 3.64: Comparison of Analytical, Numerical, and Experimental absolute pressure head traces at siphon top: H=0.3m O=100%
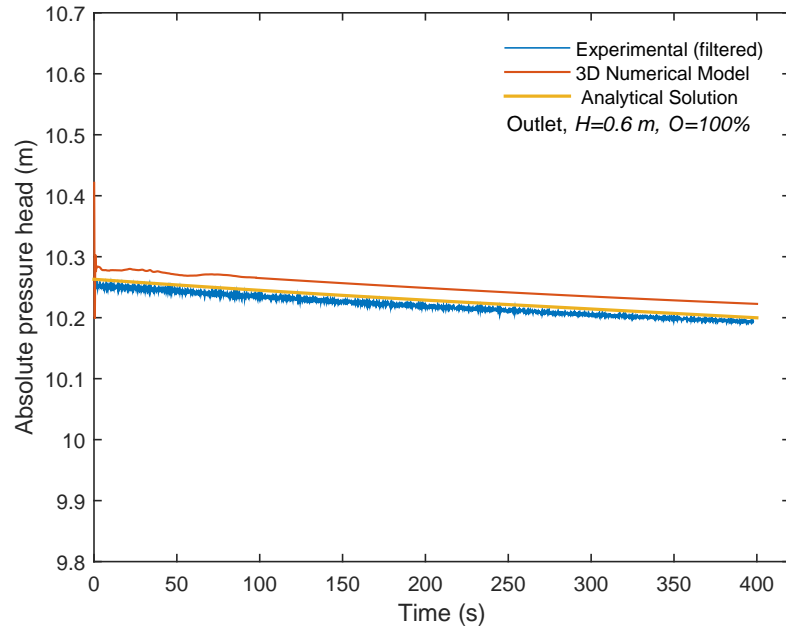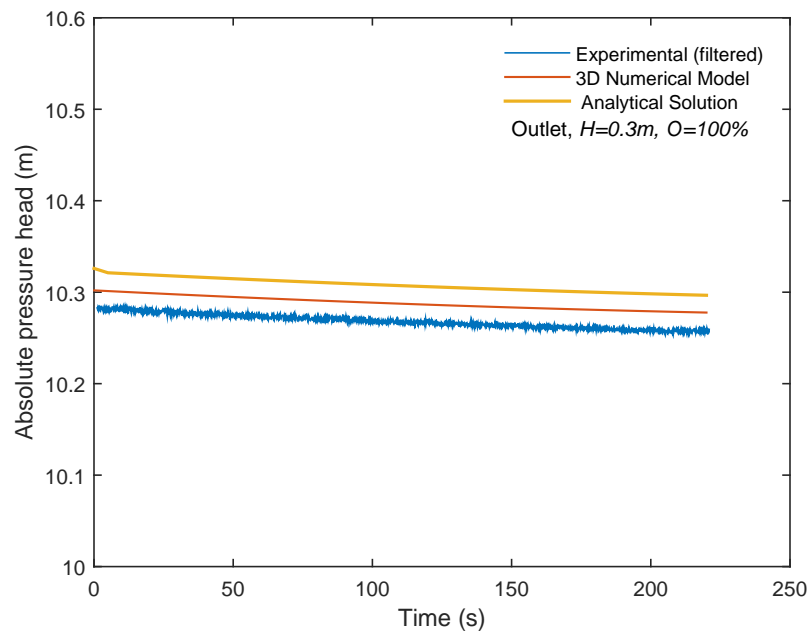

Figure 3.65: Comparison of Analytical, Numerical, and Experimental absolute pressure
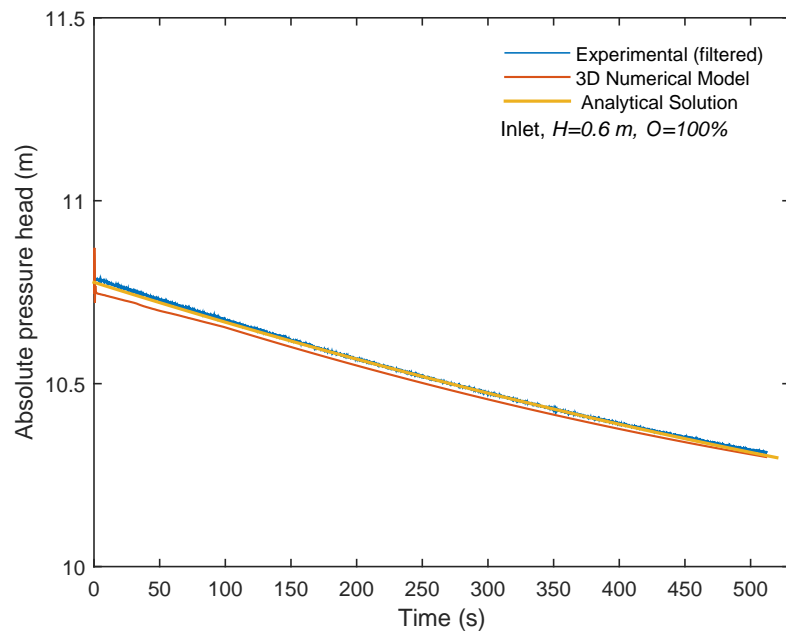
head traces at siphon outlet: H=0.3m O=100%
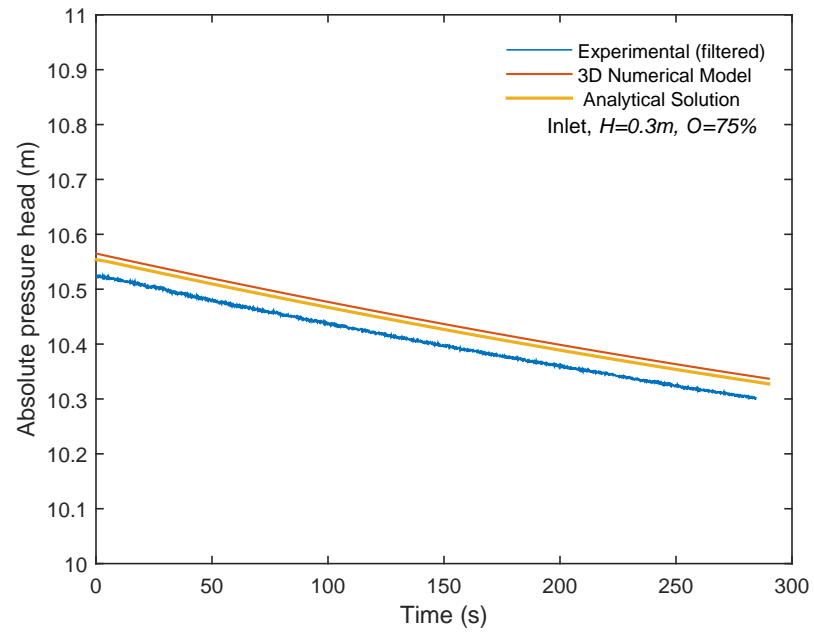
Figure 3.66: Comparison of Analytical, Numerical, and Experimental absolute pressure head traces at siphon inlet: H=0.3m O=75%
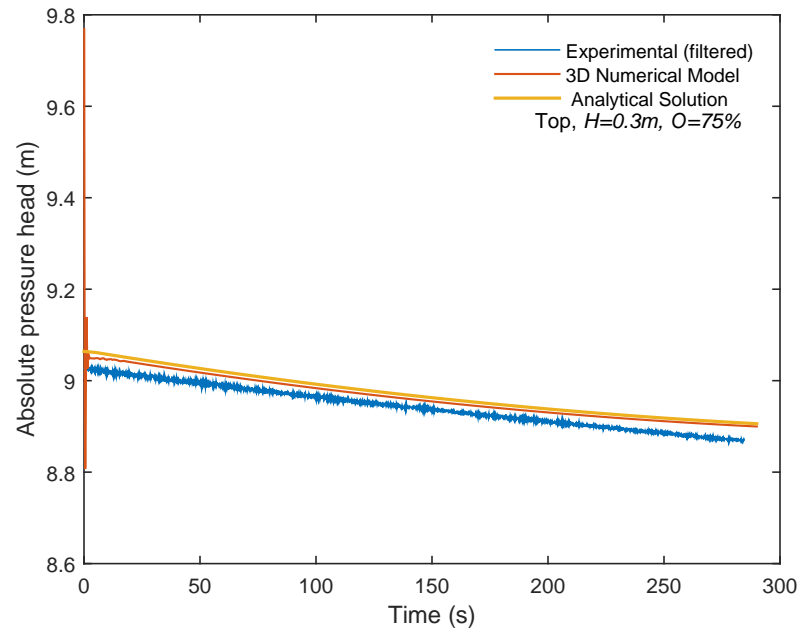
Figure 3.67: Comparison of Analytical, Numerical, and Experimental absolute pressure head traces at siphon top: H=0.3m O=75%
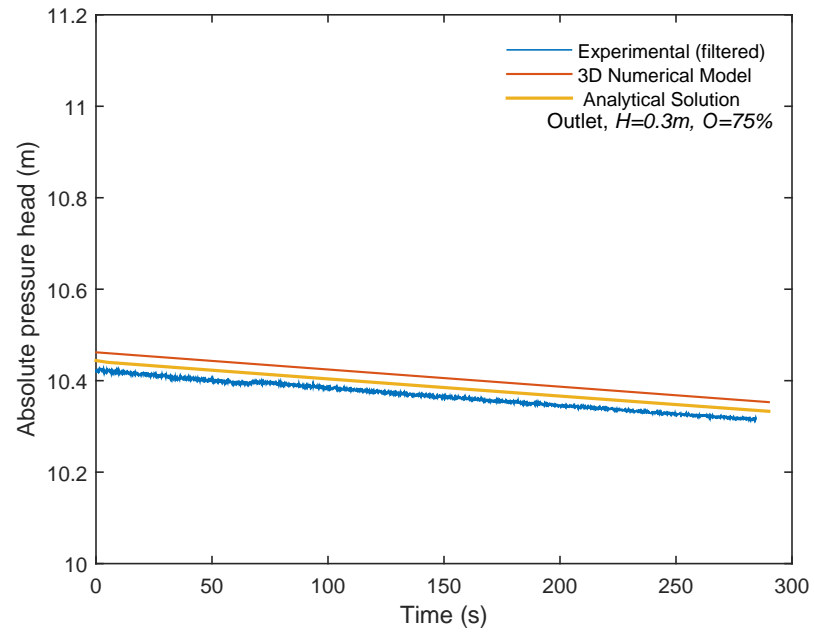
Figure 3.68: Comparison of Analytical, Numerical, and Experimental absolute pressure head traces at siphon outlet: H=0.3m O=75%
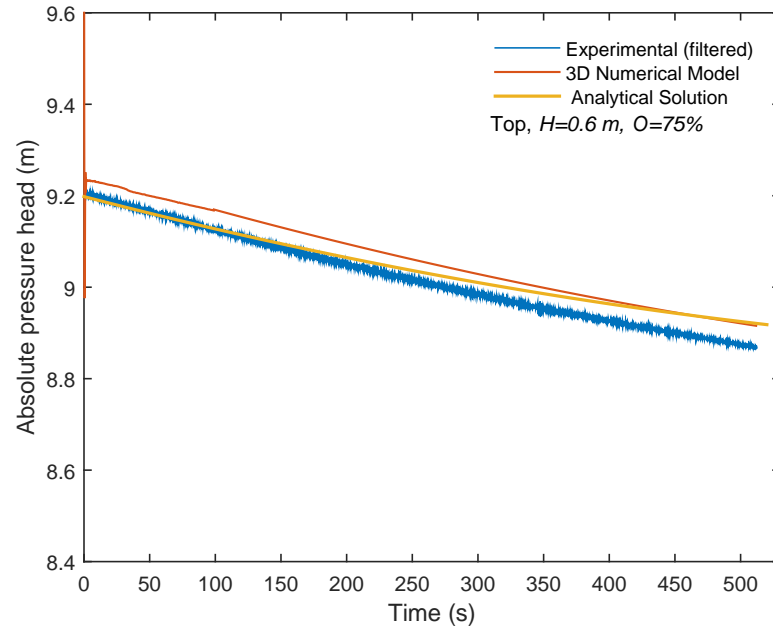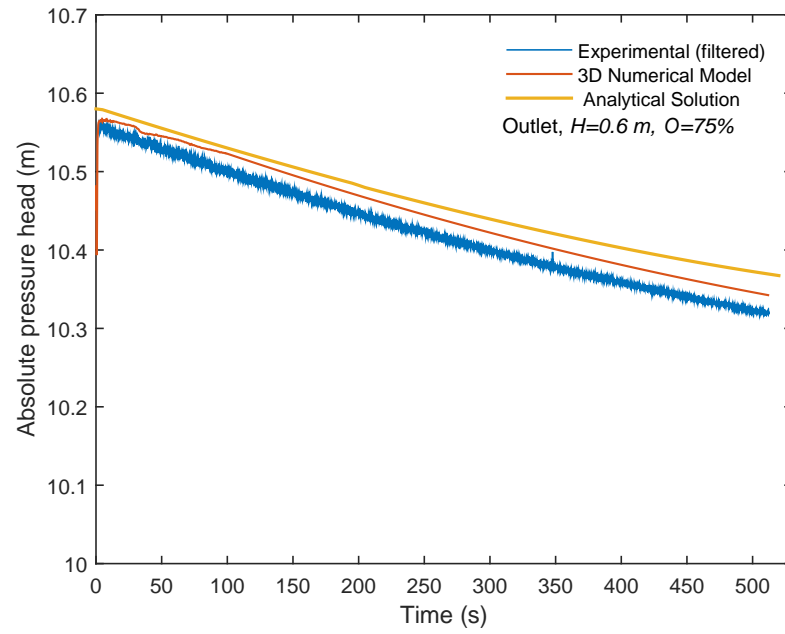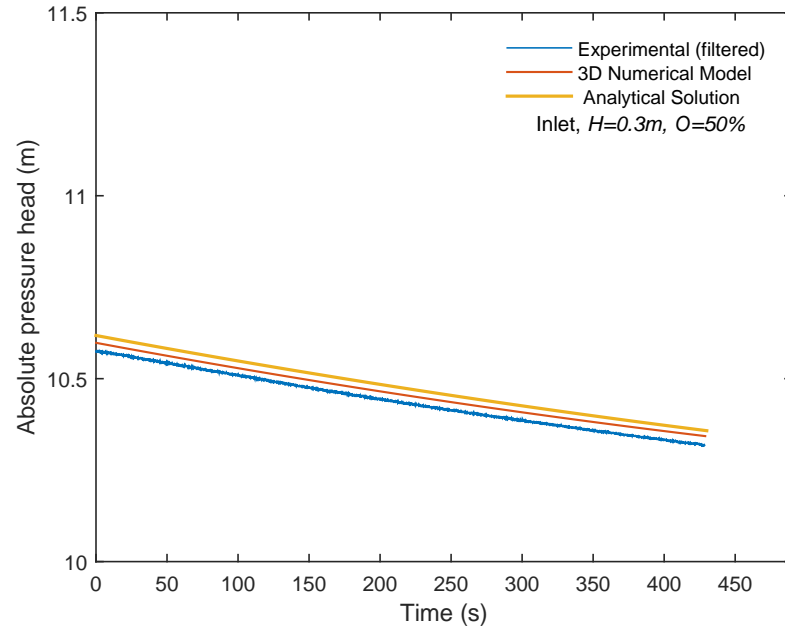
Figure 3.69: Comparison of Analytical, Numerical, and Experimental absolute pressure head traces at siphon inlet: H=0.3m O=50%
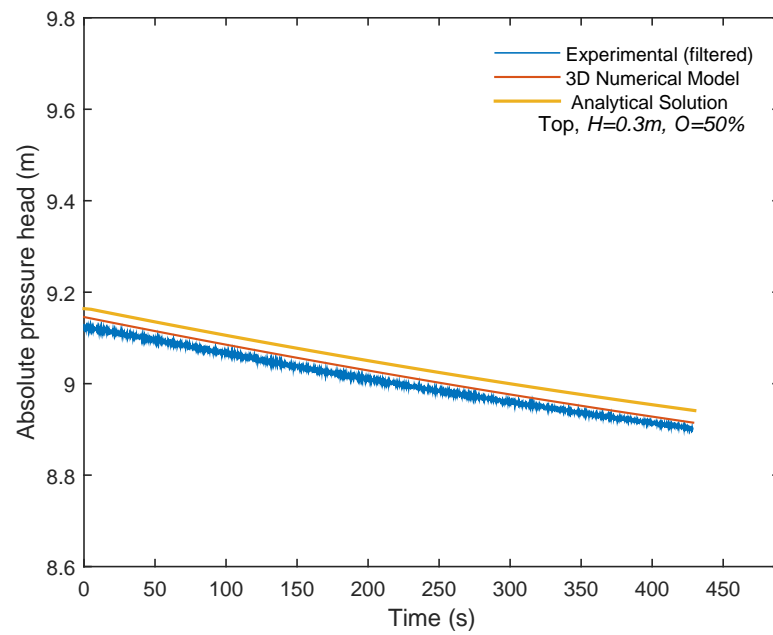
Figure 3.70: Comparison of Analytical, Numerical, and Experimental absolute pressure head traces at siphon top: H=0.3m O=50%
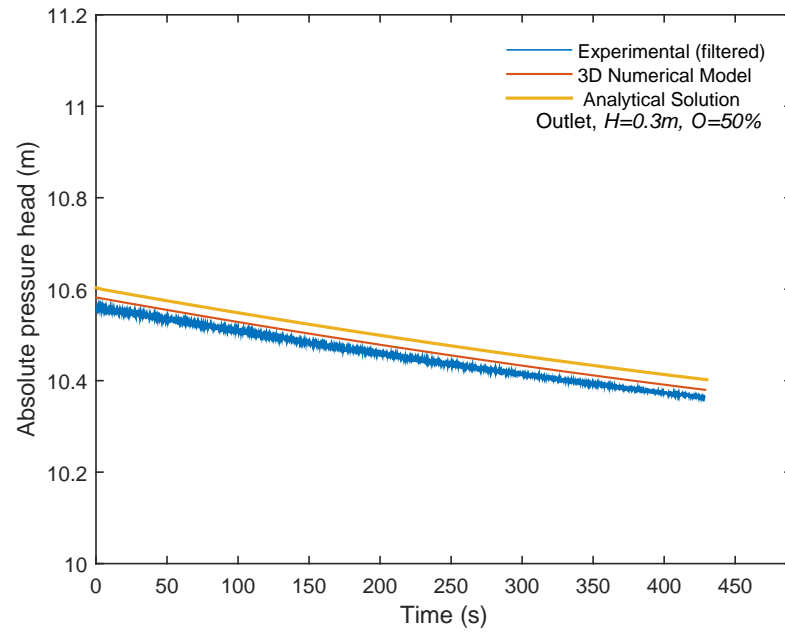
Figure 3.71: Comparison of Analytical, Numerical, and Experimental absolute pressure head traces at siphon outlet: H=0.3m O=50%
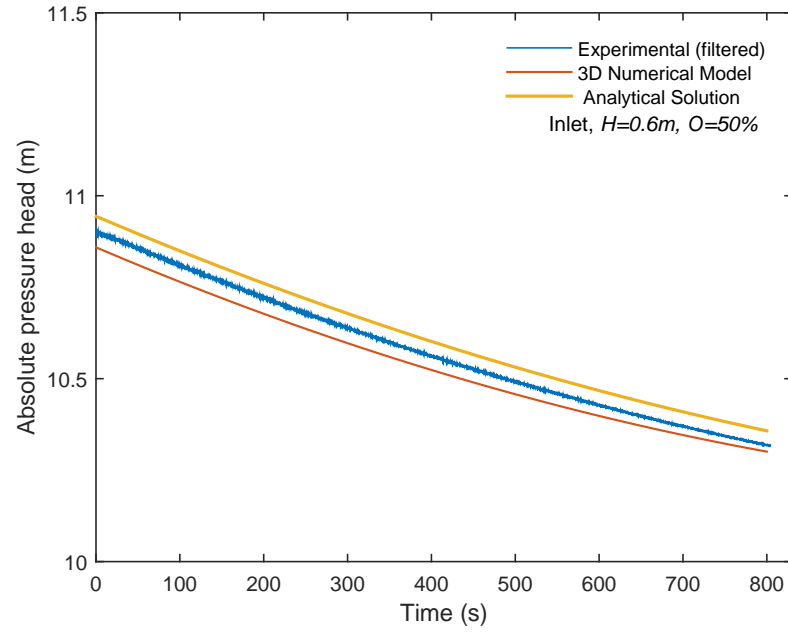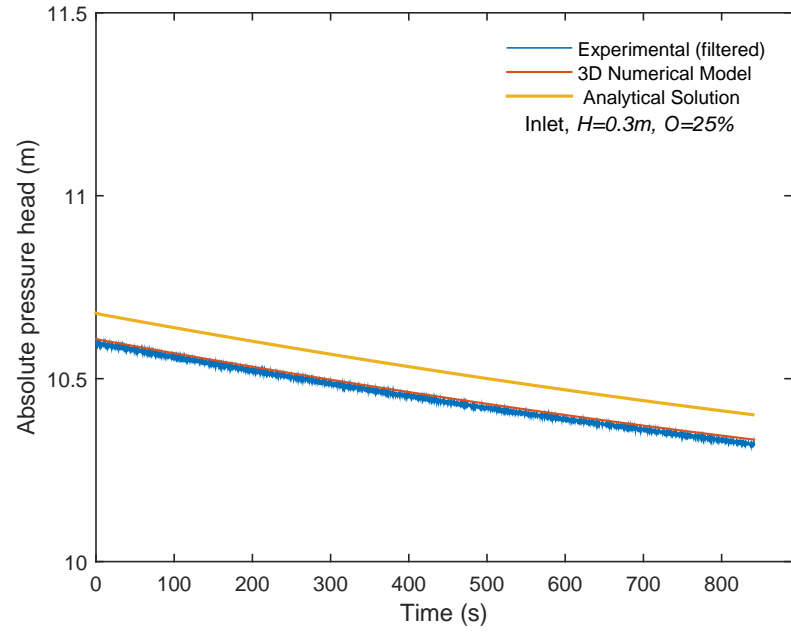
Figure 3.72: Comparison of Analytical, Numerical, and Experimental absolute pressure head traces at siphon inlet: H=0.3m O=25%
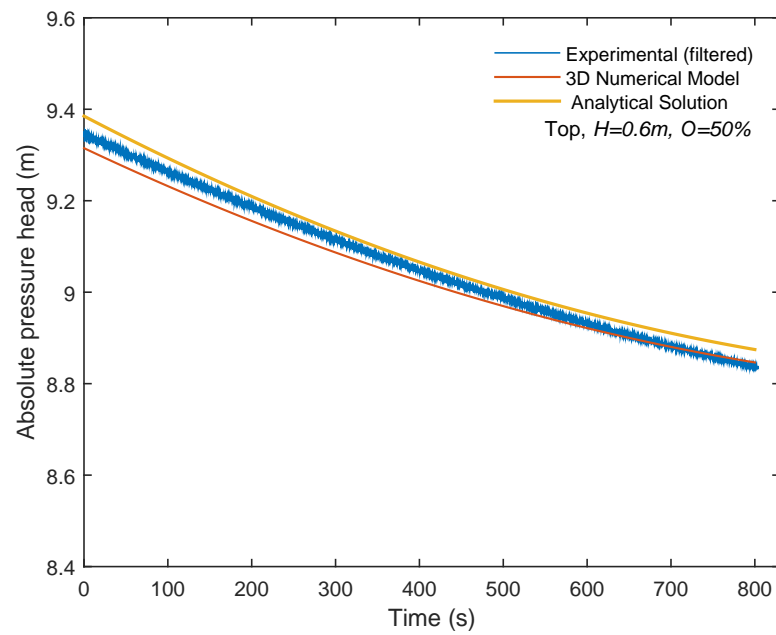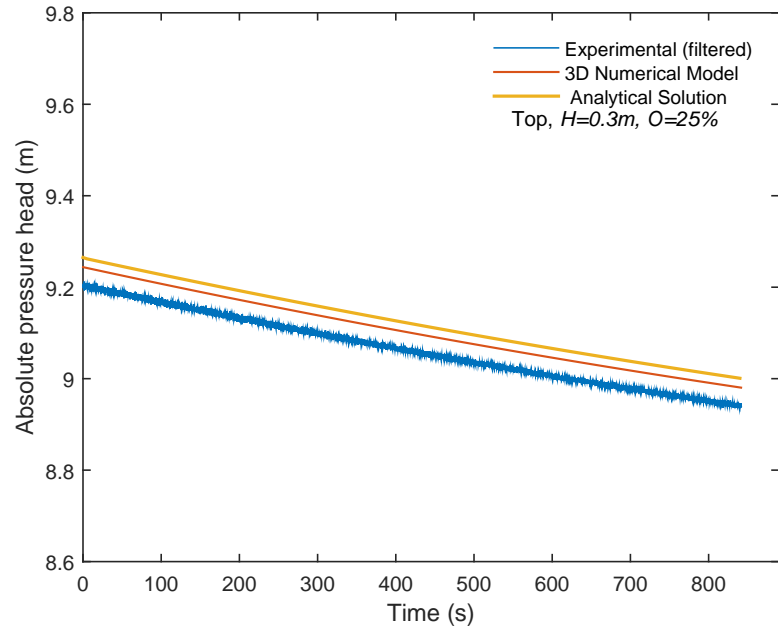
Figure 3.73: Comparison of Analytical, Numerical, and Experimental absolute pressure head traces at siphon top: H=0.3m O=25%
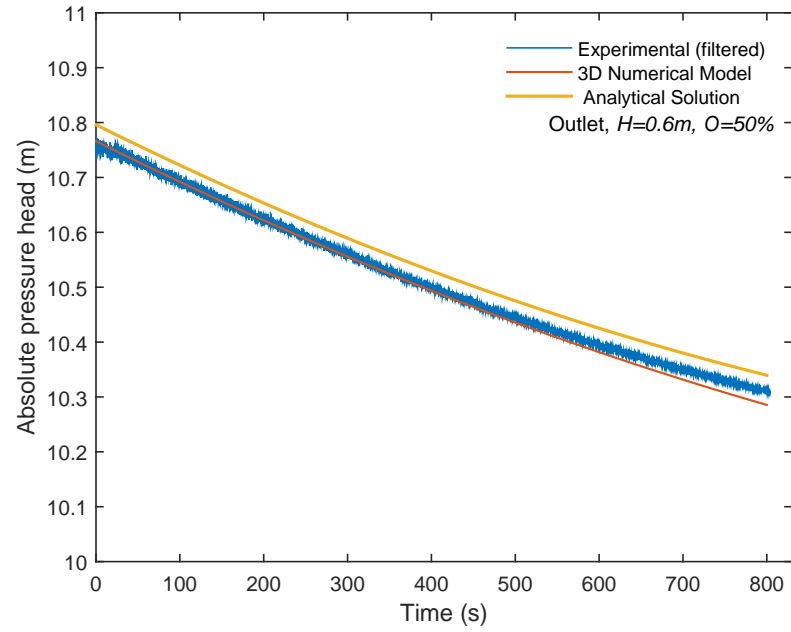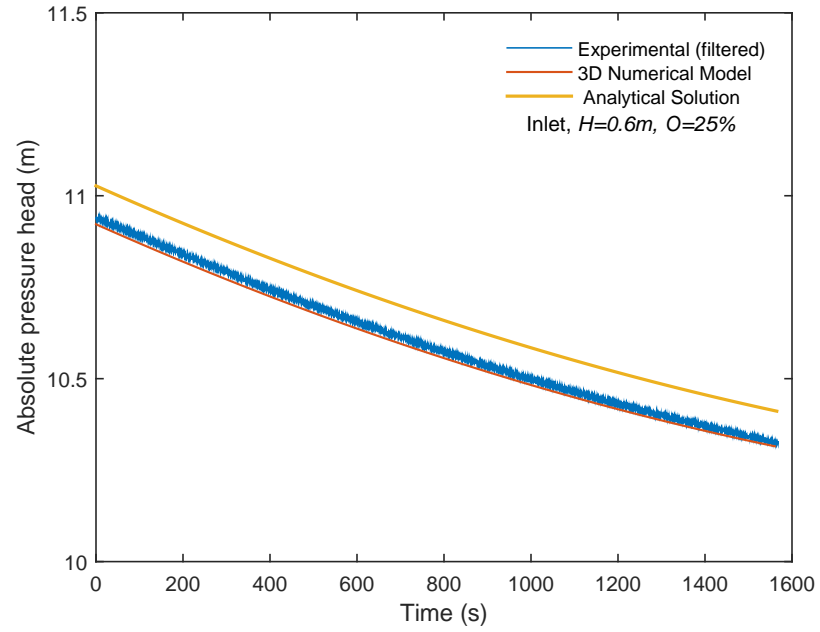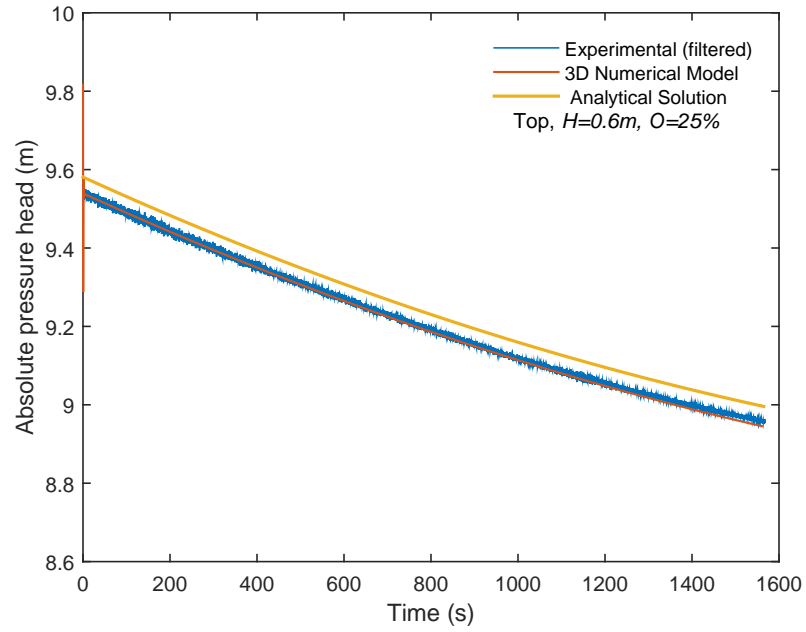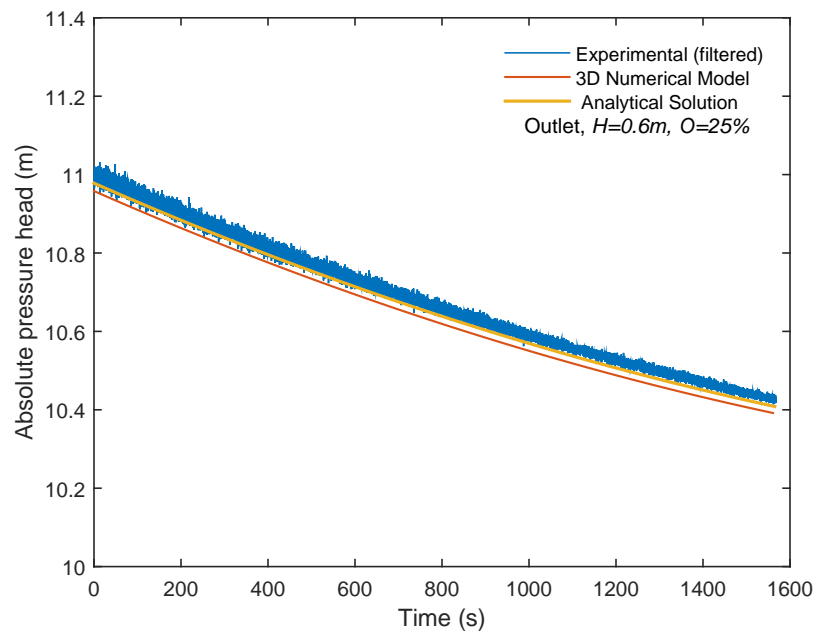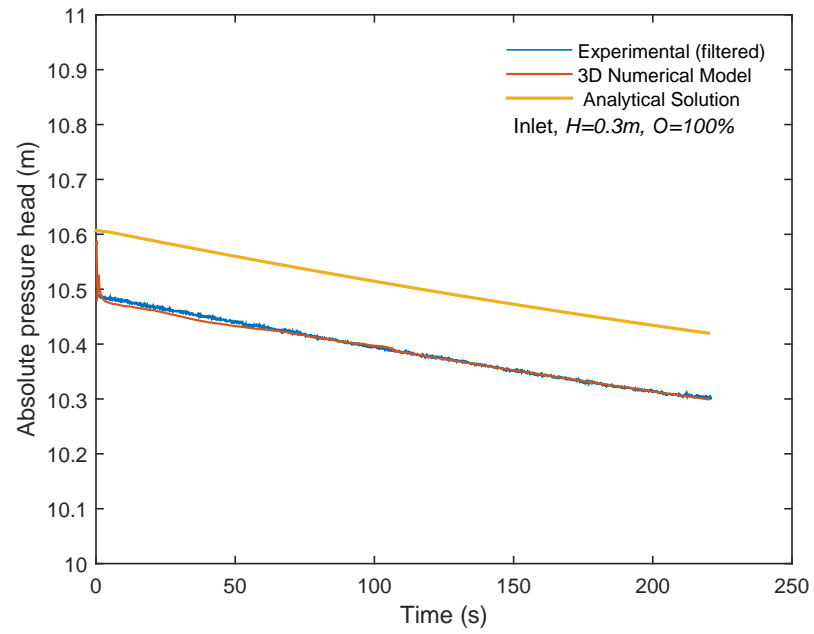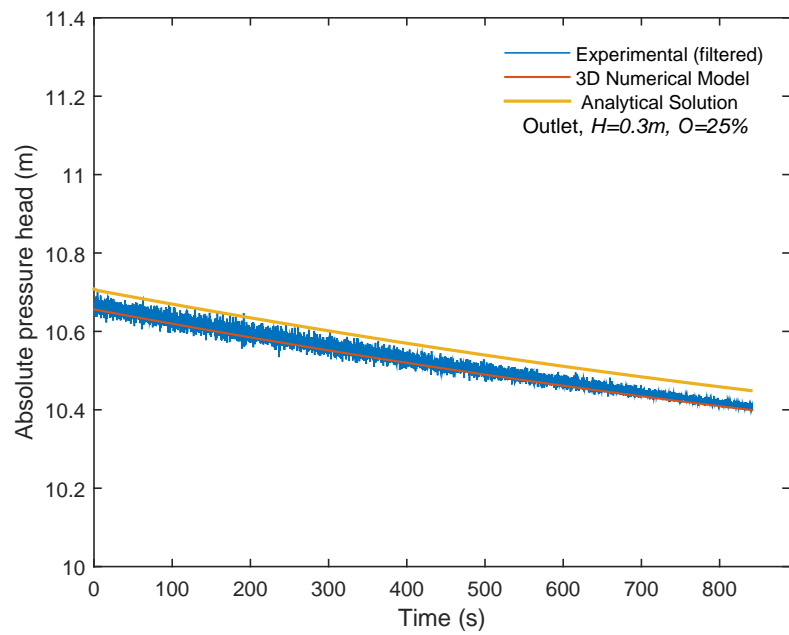

Figure 3.74: Comparison of Analytical, Numerical, and Experimental absolute pressure head traces at siphon outlet: H=0.3m O=25%

Chapter 4: Conclusion

1. The initiation of flows in a siphon with a downstream ball valve for a rapid and gradual openings were studied analytically, numerically, and experimentally. Three initial water levels in the upstream tank and four different final positions for the valve openings were studied. Two opening times of the valve were also investigated.

2. In general, good agreement between analytical, experimental and numerical results were obtained.

3. The siphon system was found to initiate the flow regardless the downstream valve is opened rapidly or gradually. However, small leakages may lead to air at atmospheric pressure to rush into the top of the siphon and stop the flow.

   Overall, the proposed siphon system could be an effective and inexpensive method to dynamically manage the storage of ponds and wetlands for flood control. However, each project site may have specific challenges that need to be considered. For example, site specific grade limitations may influence the performance of a siphon since siphons are limited to approximately 6 m of lift at mean sea level. Also, the inlet of a siphon must be designed to prevent air and sedimentation from entering to the pipe.

Bibliography

Babbar-Sebens, M., Barr, R. C., Tedesco, L. P., and Anderson, M. (2013). Spatial identification and optimization of upland wetlands in agricultural watersheds. *Ecological Engineering*, 52(0):130 – 142.

Bekele, E. G. and Nicklow, J. W. (2007). Multi-objective automatic calibration of swat using nsga-ii. *Journal of Hydrology*, 341(3):165–176.

Binder, P.-M. and Richert, A. (2011). The explicit siphon. *Physics Education*, 46(6):710–711.

Boatwright, J. (2014). Air-regulated siphon spillways: Performance, modeling, design, and construction.

Bomont, S. (2008). Back experience of deep drainage for landslide stabilization through lines of siphon drains and electro-pneumatics drains: a french railway slope stabilization example. *Chen, JY, Zhang, JM, Li, ZK, et al*, pages 1713–1720.

Breckpot, M., Blanco, T. B., and De Moor, B. (2010). Flood control of rivers with nonlinear model predictive control and moving horizon estimation. In *Decision and Control (CDC), 2010 49th IEEE Conference on*, pages 6107–6112. IEEE.

Bryant, S. (1996). Analysis of siphon lake drain performance for a small earthen dam. page 12.

Buss, L. S. (2005). Nonstructural flood damage reduction within the us army corps of engineers. *Journal of Contemporary Water Research & Education*, 130(1):26–30.

Cai, Y.-l., Sun, H.-y., Shang, Y.-q., and Xiong, X.-l. (2014). An investigation of flow characteristics in slope siphon drains. *Journal of Zhejiang University SCIENCE A*, 15(1):22–30.

Cambiaghi, A. and Schuster, R. (1989). Landslide damming and environmental protection–a case study from northern italy. In *Proceedings of 2nd International Symposium on Environmental Geotechnology, Shanghai, China*, volume 1, pages 381–385.

CD-adapco (2012). User guide star-ccm+ version 7.

Clark, A., Fort, D., Holliday, J., Gillarduzzi, A., and Bonmont, S. (2007). Allowing for climate change; an innovative solution to landslide stabilisation in an environmentally sensitive area on the isle of wight. *Mathie, E., McInnes, R., Fairbank, H., et al*, pages 443–454.

Cole, C. A., Brooks, R. P., and Wardrop, D. H. (1997). Wetland hydrology as a function of hydrogeomorphic (hgm) subclass. *Wetlands*, 17(4):456–467.

Costanza, R., Farber, S. C., and Maxwell, J. (1989). Valuation and management of wetland ecosystems. *Ecological economics*, 1(4):335–361.

De Bruijn, K., Klijn, F., McGahey, C., Mens, M., and Wolfert, H. (2008). Long-term strategies for flood risk management: scenario definition and strategic alternative design. *FLOODsite Consortium, T14_08_01*.

EPA (1996). Why watersheds. Technical report, Environmental Protection Agency. EPA800-F-96-001.

Erwin, K. L. (2009). Wetlands and global climate change: the role of wetland restoration in a changing world. *Wetlands Ecology and management*, 17(1):71–84.

Garrett, R. E. (1991). Principles of siphons. *Journal of the World Aquaculture Society*, 22(1):1–9.

Godschalk, D. (1999). *Natural hazard mitigation: Recasting disaster policy and planning*. Island Press.

Govi, M. (1989). The 1987 landslide on mount zandila in the valtellina, northern italy. *Landslide News*, 3:1–3.

Granger, R. A. (1995). *Fluid Mechanics*. Dover Publications, New York.

Haaland, S. (1983). Simple and explicit formulas for the friction factor in turbulent pipe flow. *Journal of Fluids Engineering*, 105(1):89–90.

Hey, D. L. and Philippi, N. S. (1995). Flood reduction through wetland restoration: the upper mississippi river basin as a case history. *Restoration Ecology*, 3(1):4–17.

Holloway, J. L. (1958). Smoothing and filtering of time series and space fields. *Advances in geophysics*, 4:351–389.

Hughes, S. W. (2010). A practical example of a siphon at work. *Physics Education*, 45(2):162.

Hwang, S.-B., Korenbrot, J. I., and Stoeckenius, W. (1977). Proton transport by bacteriorhodopsin through an interface film. *The Journal of membrane biology*, 36(1):137–158.

ICE (2002). Learning to live with rivers. Report, Institution of Civil Engineers (ICE), London, UK.

Jones, W. and Launder, B. (1973). The calculation of low-reynolds-number phenomena with a two-equation model of turbulence. *International Journal of Heat and Mass Transfer*, 16(6):1119–1130.

La Stabilsiation, R. D. S., De Glissements, D., and Slovaquie, T. P. D. S. E. (2013). Experience with drainage and ground stabilisation by siphon drains in slovakia. In *Proceedings of the 5th International Young Geotechnical Engineers' Conference: 5th IYGEC 2013*, volume 2, page 36. IOS Press.

Lamothe, D.-N., Neveu, G., Görlach, B., and Interwies, E. (2005). Evaluation of the impact of floods ad associated protection policies.

Lemke, D. and Richmond, S. (2009). Iowa drainage and wetlands landscape systems initiative. *Farm Foundation Competition named:The.*

Leumas, J. (1998). To siphon or not to siphon: That is the question (among others) a repair history of the crossgate dam, raleigh, north carolina. *Physics Education*, 46.

Lombardi, T. (1996). Technical review: Siphon an economic lake drain option. *ASDSO*.

Mays, L. W. (1996). *Water resources handbook*. McGraw-Hill.

Mitsch, W. J. and Day, J. W. (2006). Restoration of wetlands in the mississippi–ohio–missouri (mom) river basin: Experience and needed research. *Ecological Engineering*, 26(1):55–69.

Morrison-Maierle, I. (2012). Guidelines for use of pumps and siphons for emergency reservoir drawdown. *Montana Dept. of Natural Resources and Conservation.*

Mrvik, O. and Bomont, S. (2012). Experience with treatment of road structure landslides by innovative methods of deep drainage. *Landslides,()*, pages 79–90.

Newman, F. H. and Searle, V. H. L. (1949). general properties of matter.

Newson, M. (1997). *Land, Water and Development: Sustainable Management of River Basin Systems*. Dunod, Routledge London.

NHC (1997). Assessing losses and costs over the last 20 years. Report, National Hurricane Center (NHC).

NWS (2013). May 2013 oklahoma tornadoes and flash flooding. Report, National Weather Service (NWS), Silver Spring, Maryland.

Potter, A. and Barnes, F. (1971). The siphon. *Physics Education*, 6(5):362.

Roache, P. J. (1997). Quantification of uncertainty in computational fluid dynamics. *Annual Review of Fluid Mechanics*, 29(1):123–160.

Shih, T.-H., Liou, W. W., Shabbir, A., Yang, Z., and Zhu, J. (1995). A new k- eddy viscosity model for high reynolds number turbulent flows. *Computers & Fluids*, 24(3):227–238.

UNDP and UNISDR (2006). Integrating disaster risk reduction and climate change adaptation into ecosystem management of coastal and marine areas in south asia. Technical report, UNDP.

Van Schijndel, S. (2006). The planning kit, a decision making tool for the rhine branches. In *Floods, from Defence to Management: Symposium Proceedings of the 3rd International Symposium on Flood Defence, Nijmegen, The Netherlands, 25-27 May 2005, Book+ CD-ROM*, page 299. CRC Press.

Van Sint Annaland, M., Deen, N., and Kuipers, J. (2005). Numerical simulation of gas bubbles behaviour using a three-dimensional volume of fluid method. *Chemical Engineering Science*, 60(11):2999–3011.

Versteeg, H. and Malalasekera, W. (2007). An introduction to computional fluid dynamics: The finite volume method.

Wharton, C. (1970). The southern river swamp-a multiple use environment. school of business administration, georgia state university. *Atlanta, Georgia, USA*.

Yongfang, Z. and Yingjun, Z. (1999). Research on siphon drainage application technology [j]. *China Railway Science*, 3:006.

Zhang, Y. and Zhang, C. (1999). Experimental study of siphon drainage in xiangqian line k93 road cutting landslide. *Subgrade Engineering*, 4:26–30.